NASA Technical Paper 2874

November 1988

A Piloted Evaluation of an Oblique-Wing Research Aircraft Motion Simulation With Decoupling Control Laws

Robert W. Kempel, Walter E. McNeill, Glenn B. Gilyard, and Trindel A. Maine

NASA

NASA Technical Paper 2874

1988

A Piloted Evaluation of an Oblique-Wing Research Aircraft Motion Simulation With Decoupling Control Laws

Robert W. Kempel, Walter E. McNeill, Glenn B. Gilyard, and Trindel A. Maine
Ames Research Center
Dryden Flight Research Facility
Edwards, California

National Aeronautics and Space Administration

Scientific and Technical Information Division

CONTENTS

ABSTRACT

The NASA Ames Research Center developed an oblique-wing research airplane from NASA's F-8 digital-fly-by-wire airplane. Oblique-wing airplanes show large cross-coupling in control and dynamic behavior which is not present in conventional symmetric airplanes and must be compensated for to obtain acceptable handling qualities. The large vertical motion simulator at NASA Ames-Moffett was used in the piloted evaluation of a proposed flight control system designed to provide decoupled handling qualities. Five discrete flight conditions were evaluated ranging from low altitude subsonic Mach numbers to moderate altitude supersonic Mach numbers.

The flight control system was effective in generally decoupling the airplane. However, all participating pilots objected to the high levels of lateral acceleration encountered in pitch maneuvers. In addition, the pilots were more critical of left turns (in the direction of the trailing wingtip when skewed) than they were of right turns due to the tendency to be rolled into the left turns and out of the right turns. Asymmetric sideforce as a function of angle of attack was the primary cause of lateral acceleration in pitch. Along with the lateral acceleration in pitch, variation of rolling and yawing moments as functions of angle of attack caused the tendency to roll into left turns and out of right turns.

INTRODUCTION

Oblique-wing airplanes have advantages for many missions, both military and civilian. For missions that require both long subsonic range and endurance and a good supersonic dash capability, an oblique-wing design will have lower wave drag, lower structural weight, and reduced ground storage area when compared with other variable geometry configurations. Analytic studies, wind tunnel tests, and low-speed lightweight aircraft flight tests have been conducted, but as yet no high-performance demonstrator or operational aircraft has been developed due to the high risk inherent in such a departure from conventional designs (Gregory, 1985). Recent advances in composite structural technology make it possible to tailor oblique-wing panels for multiple flight-operating conditions while retaining the weight advantages of new materials.

The NASA Ames Research Center, Moffett Field (Ames-Moffett) and Dryden Flight Research Facility (Ames-Dryden), Edwards, California, in conjunction with the U. S. Navy, developed an oblique wing research airplane (OWRA) demonstrator (Holt, 1985). NASA's F-8 digital-fly-by-wire airplane was modified for the oblique-wing configuration. As a major part of this program, the primary flight control system will be synthesized to provide both acceptable vehicle stabilization and handling qualities across the Mach number–altitude, angle of attack, and wing skew flight envelope.

The advantages of an oblique wing cannot be obtained without overcoming many design challenges. Oblique-wing airplanes show large cross-coupling in control response and dynamic behavior which is not present in conventional symmetric airplanes. The open-loop cross-coupling of the OWRA is characterized as a relatively large roll and lateral acceleration coupling with pitch command inputs and pitch coupling with roll command inputs; all are functions of wing skew, angle of attack, Mach number, and altitude (Curry and Sim, 1983; 1984; Sim and Curry, 1984; 1985) . Therefore, it is a primary requirement that the flight control system provide decoupling so that good stability and handling qualities are achieved across the flight envelope.

To evaluate a proposed flight control system for the OWRA, the vertical motion simulator (VMS) at NASA Ames-Moffett was used. The goals of this investigation were as follows: to obtain preliminary pilot evaluations of a prototype flight control system designed to provide decoupled handling qualities; to identify important response variables in the evaluation of this unusual configuration; and to develop criteria and requirements for use in future control laws for highly coupled airplanes. The VMS provided a unique capability to investigate the OWRA dynamic characteristics early in the control system design phase in conjunction with realistic large motion and visual simulation systems.

Six pilots participated in the VMS evaluation of the OWRA at five discrete flight conditions ranging from low altitude subsonic Mach numbers to moderate altitude supersonic Mach numbers. Each pilot was required to perform a variety of maneuvers and tasks and to provide both written and oral comments with numerical pilot ratings. The control law was a prototype sys-

tem based on the loop-shaping approach (Enns, 1985; Enns and others, 1987) with the specific objectives of decoupling the longitudinal and lateral-directional motions of the aircraft and to satisfy conventional flight control objectives, including gust attenuation, stability augmentation, good command tracking, good handling qualities, and stability robustness with respect to model uncertainty. This control law did not use gain scheduling; therefore, all flights were flown at fixed wing skew and were limited to relatively small variations in Mach number, altitude, and angle of attack about each design point.

The results of this evaluation should be considered preliminary and not necessarily characteristic of a final OWRA configuration or typical of an operational oblique-wing configuration. The preliminary aerodynamic data base used in this investigation was for a wing area that was only 67 percent of the most recent OWRA wing design. Since the cross-coupling is largely dependent on the angle-of-attack change required for maneuvering, the increased wing area would be expected to result in improved aerodynamic characteristics (that is, somewhat reduced coupling) compared with the data base used in this study. In addition, the five flight conditions selected for evaluation were at moderate to high dynamic pressures which would tend to aggravate unusual dynamic characteristics.

NOMENCLATURE

All coefficients, derivatives, and moments and products of inertia are referenced to the body axes. Wing skew is the angle between the straight chord line on the wing and the vehicle Y-Z plane. A zero subscript indicates an initial condition value.

ADI	attitude-direction indicator
AR	wing aspect ratio, b^2/S
$A(y/n)$	side-acceleration parameter
$\tilde{a}_y$	control law directional regulated variable, g
$\tilde{a}_z$	control law pitch regulated variable, g
b	reference wing span, ft
$\bar{c}$	reference chord, ft
c.g.	center of gravity, in percent of $\bar{c}$
CGI	computer-generated image
CIOU	computer input–output unit
CP-V	control program–five
DFBW	digital fly by wire
g	acceleration due to gravity, ft/sec^2
Hz	unit of frequency, hertz (cycles/sec)
h	altitude, ft
M	Mach number
m	vehicle mass, slugs
OWRA	oblique wing research airplane
$\tilde{p}$	control law roll regulated variable, rad/sec
PR	pilot rating
$\bar{q}$	dynamic pressure, lb/ft^2
RIOU	remote input–output units
RMS	root mean square
S	reference wing area, ft^2
s	Laplace transform variable
t	time, sec
TED	trailing edge down
TER	trailing edge right
u_1	total roll input command, rad/sec
u_2	total directional input command, g
u_3	total pitch input command, g
V	true airspeed, ft/sec
V_e	equivalent airspeed, knots
V_0	true initial airspeed, ft/sec
VMS	vertical motion simulator
X	vehicle longitudinal body axis
Y	vehicle lateral body axis
y_i	proportional command output, rad
y_i'	integral command output, rad/sec
Z	vehicle vertical body axis
α	angle of attack, deg

β	angle of sideslip, deg
θ	pitch Euler angle, deg or rad
ϕ	roll Euler angle, deg or rad
ψ	yaw Euler angle, deg or rad
Δ	increment from reference, ft
δ_a	aileron deflection (positive for right roll), deg; $\delta_a = (\delta_{aL} - \delta_{aR})$
δ_{aL}	left aileron position (positive for TED), deg or rad
δ_{aR}	right aileron position (positive for TED), deg or rad
δ_{DT}	differential horizontal stabilizer deflection (positive for right roll), deg; $\delta_{DT} = (\delta_{eL} - \delta_{eR})$
δ_{ES}	pilot's pitch stick position (positive for stick aft), in.
δ_e	symmetric horizontal stabilizer deflection, deg (positive for TED); $\delta_e = (\delta_{eL} + \delta_{eR})/2$
δ_{eL}	left horizontal stabilizer position (positive for TED), deg or rad
δ_{eR}	right horizontal stabilizer position (positive for TED), deg or rad
δ_{LS}	pilot's lateral stick position (positive for right stick), in.
δ_{RP}	rudder pedal deflection (positive for right pedal forward), in.
δr	rudder deflection (positive for TEL), deg or rad
Λ	wing skew angle (positive for right wing forward), deg

Control Law Gains and Filter Coefficients

a_i	lead compensation parameter, rad/sec
b_i	actuator compensation parameter, rad/sec
c_i	lead compensation parameter
f	a_y compensation parameter, rad/sec
h	a_y compensation parameter, rad/sec
H_1	rudder pedal precompensation parameter
H_2	longitudinal stick precompensation parameter
H_{ij}	integral gain
K_{ij}	proportional gain
p_1	rudder pedal precompensation parameter, rad/sec
p_2	longitudinal stick precompensation parameter, rad/sec

Coefficients

C_l	rolling moment
C_n	yawing moment
C_Y	sideforce

Linearized Dimensional Aerodynamic Derivatives

L_α	change in rolling acceleration due to change in angle of attack, sec^{-2} (element $A_{6,2}$ of the state matrix)
L_β	effective dihedral, sec^{-2} (element $A_{6,3}$ of the state matrix)
N_α	change in yawing acceleration due to change in angle of attack, sec^{-2} (element $A_{8,2}$ of the state matrix)
Y_α	change in sideforce due to change in angle-of-attack derivative (Y/mV) in the $\dot{\beta}$ equation, sec^{-1} (element $A_{3,2}$ of the state matrix)
Y_β	sideforce derivative in the $\dot{\beta}$ equation, sec^{-1} (element $A_{3,3}$ of the state matrix)

Matrix Format of the State Space Models

A	state matrix of the state equation, $C\dot{x} = Ax + Bu$
B	control matrix of the state equation
C	C matrix of the state equation

Body Axis Moments of Inertia (all inertias are slug-ft^2)

I_{xx}	roll moment

I_{xy}	roll-pitch cross product
I_{xz}	roll-yaw cross product
I_{yy}	pitch moment
I_{yz}	pitch-yaw cross product
I_{zz}	yaw moment

Body Axis Angular Rates

p	roll, deg/sec or rad/sec
q	pitch, deg/sec or rad/sec
r	yaw, deg/sec or rad/sec

Body Axis Translational Accelerations

a_n	normal acceleration at the c.g., g
a_{nP}	normal acceleration at the pilot's station, g
a_y	lateral acceleration at the c.g., g
a_{yP}	lateral acceleration at the pilot's station, g

Sign Convention

All parameters are referenced to a right-hand axis system with origin at the vehicle center of gravity. Positive directions are as follows: forward (X axis), out the right wing (Y axis), and down (Z axis). All attitudes and angular rates are positive in a clockwise rotation about the appropriate axis. Angle of attack is positive when the X-body axis is above the velocity vector. Angle of sideslip is positive when the X-body axis is to the left of the velocity vector.

AIRPLANE DESCRIPTION

The oblique-wing research airplane (OWRA) considered for this simulation consists of a modification to NASA's F-8 digital-fly-by-wire (DFBW) airplane. The current variable incidence high wing would be replaced by a variable skew wing and pivot assembly. The existing all-moving F-8 horizontal stabilizer would be modified to operate differentially for roll control.

Basic F-8 Digital-Fly-By-Wire Airplane

Physical characteristics

The F-8 DFBW airplane was modified from a U.S. Navy F-8C Crusader carrier-based fighter. The F-8C airplane is of mid-1950s vintage, a high-wing, single engine configuration capable of supersonic speeds up to Mach1.8 and altitudes to 60,000 ft. The airplane is a swept-wing configuration with a swept-vertical tail, and an all movable swept-horizontal stabilizer. The engine is a J57-P420 turbojet with afterburner. The weight of the F-8 DFBW airplane ranged from approximately 18,800 lb empty to a maximum of 27,400 lb. The wing is mounted high on the fuselage and uses variable incidence for landing and takeoff. Aerodynamic controls consist of aileron–flaps for roll control, horizontal stabilizer for pitch control, rudder for yaw control. Dimensions and physical characteristics are given in table 1.

Flight control system

The flight control system (Szalai and others, 1978) has been extensively modified to provide a digital-fly-by-wire flight control system. The modified flight control system included appropriate sensor sets, triplex primary and backup digital computers, interface units, and secondary actuators that provided the commanded inputs to the primary actuators. The mechanical flight control system was totally removed.

F-8 Oblique Wing Research Airplane

Physical characteristics

Planned modifications to be made to the basic airplane include a variable incidence composite wing with pivot–skew assembly, flight control computers and interfaces, and differential horizontal stabilizer. The weight of the OWRA ranges from 23,500 to an empty weight of 18,800 lb. The weight used in this simulation study was held constant at 21,116 lb which represented 50 percent fuel loading. A three-view drawing of the OWRA is shown in figure 1. The mass and center of gravity characteristics are presented in appendix A.

Aerodynamic controls

The airplane's aerodynamic controls consist of the following movable surfaces: wing ailerons for roll

control, symmetric and differential stabilizer for pitch and roll control, rudder for yaw control, and flaps. Variable wing incidence has been retained. Control surface authorities and wing aileron strategy as a function of wing skew have not been completely determined. For this study wing ailerons were not used. Dimensions and physical characteristics for the basic F-8 airplane and the OWRA configuration used in this study are presented and compared in table 1.

Wing

A complete preliminary aerodynamic model of an early design was used in this study. The wing area of this model was 200 ft^2 and incorporated a vertical pivot axis with the wing elevated slightly above the fuselage, the resulting gap being filled by a fairing. The wing pivot point was at 33.6 percent of the reference chord length. The wing was rotated about this point from 0° to 65° with the right wing forward. The proposed flight configuration, however, would incorporate a 300 ft^2 wing, a wing pivot axis cant angle that results in 0° cant at 0° skew and 10° cant at 65° skew, and would have the wing raised even more above the fuselage, with a larger fairing filling the gap. Each of these design features was expected to reduce the aerodynamic cross-coupling in the proposed flight regime; however, limited data were available for this configuration.

Flight control system

The proposed flight control system for the OWRA will include replacing the current triplex primary and triplex backup computers with a quadruplex fault-tolerant computer architecture including a software backup system. Existing sensor sets, interface units, and secondary and primary actuators will be used with modifications as required. The control law would be an entirely new design and make use of the differential horizontal stabilizer (not a normal F-8 aircraft function) for roll control at high skew angles and trim to all surfaces.

With the wing in the skewed position, asymmetric static aerodynamic forces and moments act on the wing-fuselage combination which must be trimmed out. Included in these forces is a relatively large sideforce. To maintain constant heading with the wing at some skew angle, the sideforce must be neutralized by using either sideslip, bank angle, or a combination of sideslip and bank angle (Curry and Sim 1984; Sim and Curry, 1985). In the VMS tests, only the symmetric horizontal stabilizer, differential horizontal stabilizer, and rudder were used to establish static trim for each flight condition.

VERTICAL MOTION SIMULATION DESCRIPTION

The vertical motion simulator (VMS) is a general six-degree-of-freedom large-motion simulator (fig. 2) capable of providing realistic motion and visual cues for a wide range of aircraft types, configurations, and flight conditions. The VMS provided a means of realistically evaluating the preliminary handling qualities of the unconventional OWRA configuration early in the program development. The cockpit was mounted directly on a synergistic electrohydraulic motion generator (hexapod) that provided pitch, roll, and yaw rotational degrees of freedom with limited translational degrees of freedom. Large lateral motions were generated by driving the cockpit-hexapod assembly across a movable platform by means of electric motors and a rack-and-pinion gearing arrangement. The largest degree of freedom was vertical translation. Vertical translational motion was provided to the platform through twin vertical columns driven by rack-and-pinion geared electric motors. The weight of the entire simulator assembly was counterbalanced by means of nitrogen-filled underground pressure vessels. The maximum performance characteristics of the VMS are shown in table 2.

The VMS closed loop system block diagram is presented in figure 3. The interrelationships of the various elements of the VMS facility are shown in the figure. The host digital computer, a Sigma 8 (Xerox Corp., El Segundo, California), is connected through a logic pulse unit to a PDP 11/55 (Digital Equipment Corp., Maynard, Massachusetts), which serves as the main interface between the host computer, VMS motion-generating system, VMS cockpit instruments, pilot's stick and rudder force-feel system, and data recording equipment. The Sigma 8 computed all aircraft forces, moments, velocities, and positions. The PDP 11/55, in addition to serving as the distributor of data to the various remote input–output units (RIOU) which drive the peripheral elements of the simulation, executes the VMS motion logic equations. These

equations govern the motion washouts necessary to keep the simulator within its limits of travel and the residual cockpit tilt angles required to simulate long-term longitudinal and lateral accelerations. Data for generation of the visual scene are transmitted directly from the Sigma 8 to the Perkin-Elmer digital computer (Perkin-Elmer Corp., Ocean Port, New Jersey) via a computer input–output unit (CIOU). A Singer-Link computer-generated image (CGI) visual scene generator (Singer-Link Corp., Sunnyvale, California) was used to create a visual display.

Vertical Motion Simulator Digital Computer

The host digital computer for the VMS was an XDS Sigma 8, governed by the control program–five (CP-V) operating system. This computer contained all the nonlinear aerodynamics, mass and inertia characteristics, equations of motion, engine model, and control laws. Core size was 176,000 words (for CP-V), word size was 32 bits (8-bit bytes), and execution rate was 0.6 to 0.7 million instructions/sec.

Vertical Motion Simulator Cockpit

The cockpit used in this study was configured for an experimental helicopter that was being evaluated in the VMS at the same time as the OWRA. There was no attempt to duplicate the cockpit of the proposed OWRA since this was beyond the scope of the study. A general view of the cockpit interior, including the instrument panel and stick used in this evaluation, is shown in figure 4. The instrument panel was configured with relatively conventional flight instruments and included an attitude-direction indicator (ADI), airspeed gage, Mach meter, altimeter, vertical velocity indicator, turn-and-bank indicator, angle of attack, engine rpm, and, at the lower left, wing skew angle. The stick grip was configured to that of the helicopter, but included pitch and roll trim switches for the OWRA and a trigger switch for return to the initial condition. Realistic propulsion sound and airstream noise as functions of engine rpm and airspeed, respectively, were provided for added realism and for making power changes.

The outside visual reference consisted of a four-window CGI and was presented to the pilot using color video monitors and spherical collimating mirrors. The outside scenes included a cloudless blue sky and green ground terrain with a simplified representation of Edwards Air Force Base, which could be recognized only at low altitudes, and a high-resolution image of a KC-10 tanker aircraft. The pilots were generally critical of the lack of specific detail that the ground visual display scene presented, and noted that it was impossible to sense either speed across the ground or turn rate. The field of view was approximately 154° and therefore provided good peripheral vision of the horizon.

Operating cycle time for the OWRA simulation was approximately 50 msec. Average time delays from pilot input to simulation component output were approximately 42 msec (including a special compensation algorithm (McFarland, 1988)) for the visual display, 50 msec for the instruments, strip charts, and control loaders, and 100 msec for the VMS motion commands.

Aerodynamic Data Base

The aerodynamic data base used in the OWRA was a preliminary nonlinear data set obtained from wind-tunnel tests and augmented with appropriately scaled F-8 data and computed aerodynamic characteristics. The data were nonlinear with angle of attack, Mach number, and wing skew, but not with sideslip. The angle of attack ranged from $-4°$ to $16°$. Mach numbers ranged from 0.25 to 1.6, and wing skews were $0°$, $45°$, $55°$, and $65°$. The data set did not cover all wing skews at all Mach numbers and was somewhat limited in scope, but was satisfactory for this preliminary study. Linearized state space matrices representing the open loop aerodynamic characteristics for each of the five flight conditions for 1-g trimmed flight are presented in appendix C. These matrices are referenced to the vehicle body axis system.

FLIGHT CONTROL SYSTEM DESCRIPTION

Pilot's Stick and Rudder Pedal Characteristics

The stick and rudder pedal force-feel characteristics in the VMS were provided by a variable force-feel hydraulic loading system. This system provided the ability to vary breakout force and force gradient. No attempt was made to duplicate the basic F-8 airplane pilot control characteristics, since the actual OWRA

requirements had not been determined. A set of force-feel characteristics, that was reasonable and did not detract from the simulation, was selected for the VMS study . The stick and rudder pedal characteristics and the stick dynamics used in the VMS evaluation are presented in table 3.

Stick and Rudder Pedal Gearing

The lateral stick and rudder pedal sensitivities were held constant with deflection. The lateral stick sensitivity was 0.5 (rad/sec)/in. and the rudder pedal sensitivity was 0.2 *g*/in. The longitudinal stick sensitivity was nonlinear as a function of stick position and is presented in figure 5. Note that at trim (zero stick deflection), the sensitivity curve is linear with a slope of 1 *g*/in. for up to 1.5 in. of stick deflection.

Control Law

The control law was developed by Honeywell Systems and Research Center, Minneapolis, Minnesota, using the loopshaping methodology (Enns, 1985; Enns and others, 1987) and was a multiple-input–multiple-output design incorporating proportional plus integral paths. The key closed loop flight control system design objective was to obtain decoupling among airplane pitch, roll, and yaw axes. Other design objectives included desensitization, disturbance rejection for turbulence attenuation, stability robustness for model uncertainties, and good handling qualities. For more detail on the flight control system design and design process, see Enns and others (1987).

The resulting control system design was a preliminary version of the proposed primary control law for the OWRA. The control system consisted of five single point designs at each of the five flight conditions. Each gain set was determined for 1-*g* trim, constant wing skew, Mach number, and angle of attack. These gains were changed for each flight condition and then held constant. In some of the piloted simulations, relatively large variations in *g*, Mach, and angle of attack occurred representing significant deviation from the design point. These variations did not result in any significant degradation of system performance and thus gave a good qualitative indication of robustness.

The control law incorporated a proportional plus integral compensation path (fig. 6). The control law block diagram (fig. 6) uses the Laplace variable notation, but was implemented digitally with a 20-Hz sample rate in the VMS. All filters were digitally mechanized using Tustin's transformation while the primary actuators were mechanized using difference equations.

The control law had three pilot inputs and seven aircraft motion sensor feedbacks. Symmetric stabilizer was used for pitch control, differential stabilizer for roll control, and rudder for yaw control. These surfaces were all used to achieve static trim at each of the discrete initial flight conditions. Ailerons were not used for control or trim in this study and were held at zero for all flight conditions. The pilot's control inputs were fed to precompensation filters with the rudder and pitch command filters a function of flight condition.

The pilot's control inputs consisted of conventional longitudinal and lateral stick and rudder pedals. The seven aircraft motion sensors used as feedbacks were roll, pitch, and yaw angular rates; roll and pitch Euler angles; normal acceleration; and lateral acceleration. These feedback signals were combined to form three regulated variables. The control structure was such that the lateral stick commanded the roll variable, the longitudinal stick commanded the pitch axis variable, and the rudder pedals commanded the directional variable.

The regulated variable in the roll axis consisted of the roll rate plus a small gain multiplied by the bank angle. Thus the lateral stick primarily commanded roll rate. The small gain on the bank angle stabilized the spiral mode.

In the pitch axis, the regulated variable consisted of pitch angular rate, and a combination low-pass filtered normal acceleration and pitch Euler angle. The pitch angular rate feedback was for stability augmentation. The low-pass filtered normal acceleration provided gust attenuation. The feedback of the pitch Euler angle was for stabilization of the phugoid mode.

The directional regulated variable was a blend of low passed and lead-lag compensated lateral acceleration together with a nonlinear estimate of lateral acceleration based on the feedback parameters of roll and yaw angular rates, pitch and roll Euler angles, and the trim values of velocity, angle of attack, and sideslip. This mechanization was intended to provide coordinated turns, stability augmentation, and gust alleviation.

The regulated variables were differenced with the pilot command inputs (which had been acted upon by the precompensation filters) to form error signals. These error signals were then passed to the proportional and integral gain matrices. Reflecting the cross-coupling inherent in the asymmetric oblique-wing design, these matrices generated three commands that were each a function of all three regulated variables. The outputs of the proportional gain matrix and the integral gain matrix were summed and distributed by the surface management matrix as commands to the left and right stabilizers, and the rudder. These commands were lead compensated prior to going to the actuators. The proportional and integral gain matrices, and several of the variables in the compensation filters, would be scheduled as a function of flight condition in the final flight control law configuration. For the VMS study, these matrices and variables were changed for each flight condition and then held constant. The values of the matrices and filter variables are presented in appendix B.

The control system was designed to feed back the error between the commanded and actuator ram positions into the integral gain path. This mechanization eliminates the problem of integrator windup in the presence of actuator saturations and rate limits. This loop was opened for the VMS study. This may have made the effects of actuator saturation and rate limiting more severe, but was not significant where no saturations or rate limits occurred. The control surface position limits, rate limits, and actuator transfer functions used in the VMS study are presented in table 4.

The horizontal stabilizer was required for both pitch and roll control and trim. The stabilizer operating envelope was constrained as shown in figure 7, and the commanded symmetric stabilizer could limit the achievable differential stabilizer during some maneuvers. The flight control system gives symmetric stabilizer priority over the differential requirement.

TEST MANEUVERS AND EVALUATION PROCEDURES

Flight Conditions and Maneuvers

For the VMS evaluation the OWRA was considered to be a Class IV or high-maneuverability airplane (MIL-F-8785C, 1980). However, it should be noted that some maneuvers were selected specifically to identify and even accentuate undesirable characteristics and may not be representative of typical oblique wing missions. For example, many potential applications of oblique wing configurations, such as commercial transports, do not require desirable handling qualities during the unlikely event of high-g maneuvering. Another example is the air-to-air refueling task, which, for an oblique wing, would normally be performed with the wing at 0° skew. Simulated refueling, however, provides a recognizable high-workload piloting task useful for evaluating the control laws.

The five discrete flight conditions included in this evaluation are presented in table 5. Each of the participating pilots was required to perform several maneuvers that ranged from small to large, imprecise, and precision-maneuvering flight. This evaluation included only up-and-away maneuvering with computer generated visual flight cues. Terminal tasks were beyond the scope of this evaluation. Included in these maneuvers were windup turns to 2 and 4 g, rapid and slow entry and exit to turns of various bank angles, heading changes, push-over–pull-up maneuvers, altitude changes at low and high rates of climb, climbing and descending turns, pitch and roll command tracking tasks, and pseudo in-flight refueling for station keeping only and not hookup. Atmospheric turbulence was not included as part of this evaluation. Strip-chart recordings were made of all important aircraft variables, translational accelerations, pilot's stick inputs, and control surface positions for each evaluation.

Pitch and Roll Tracking Tasks

Pitch and roll tracking tasks were presented to each of the pilots toward the end of each flight condition evaluation. The tracking tasks used in this VMS study are presented in figure 8 and are shown normalized to ± 1. The pitch task duration was 100 sec and incorporated some roll tracking during the last 25 sec. The amplitude of the pitch task was generally $\pm 10°$ with $\pm 30°$ of roll at the end. Some of the high dynamic pressure cases were flown at $\pm 5°$ of pitch. The roll task was $\pm 60°$ for all flight conditions and lasted 100 sec. These tasks were similar to those presented in Meeker and Hall (1967) and were incorporated in the evaluation for the purpose of evaluating the precision response characteristics.

The tasks were mechanized on the horizontal needle of the attitude-direction indicator (ADI) for the pitch task and the vertical needle for the roll task. These needles displayed the error between the task commanded pitch or roll Euler angle and actual pitch or roll Euler angle. Needles centered indicated zero error and the pilot inputs were in a "fly to" sense. The changing Euler angle commands were displayed to the pilots as step or ramp inputs to the needles as a function of time.

In-Flight Refueling Task

In-flight refueling was simulated using a CGI display representing a KC-10 tanker aircraft with a refueling boom and drogue. Generally, two tasks were attempted with the refueling aircraft: loose formation with the tanker, and tight formation aft of the drogue, simulating a precontact position. Actual hookup was not simulated.

Pilot Ratings and Rating Scale

A total of six pilots participated in the evaluation. However, only two of the pilots were able to fly and evaluate all five flight conditions: one pilot evaluated four flight conditions, one pilot evaluated three conditions, and two pilots evaluated two flight conditions. Each pilot was asked to comment during the course of each evaluation. These comments were tape recorded and transcribed at a later date. In addition, the pilots were asked to complete a pilot comment card following each evaluation. An example of this pilot comment card is presented in appendix D. Each of the pilots was asked to provide numerical ratings based on the Cooper-Harper handling qualities rating scale (Cooper and Harper, 1969) and comments concerning the level of handling qualities (U.S. Air Force, 1980) for the tasks performed. The Cooper-Harper pilot rating scale is shown in table 7. The military specification levels of handling qualities roughly correspond to Cooper-Harper ratings as follows: 1 to 3, level 1; 4 to 6, level 2; and 7 to 9, level 3.

Of the six participating pilots, four were civilian NASA test pilots and two were U.S. Navy test pilots. A summary of each of the pilot's experiences is presented in table 6. Of the NASA pilots, three were from Ames-Dryden and one was from Ames-Moffett. The Navy pilots were from the Naval Air Test Center, Patuxent River, Maryland.

RESULTS AND DISCUSSION

General Handling Qualities

As in any qualitative or first look airplane flight or simulation evaluation, apparent differences of opinion among pilots tend to occur. These points of view exist because there has not been sufficient opportunity to define task performance standards and objectives to resolve differences in background training, experience, perceptions, and biases. The interpretation of both oral and written comments by the various experimenters is also subjective. The VMS evaluation of the OWRA may have accentuated differences of opinion due to the unique motion characteristics of the vehicle. In the following sections, the authors present a balanced pilot consensus and, with examples, illustrate the problems and discuss the significance of each problem.

The longitudinal and lateral stick forces and harmony were considered satisfactory for all flight conditions. Longitudinal stick force per g was considered satisfactory. The rudder pedals were considered too stiff.

In order to stress the flight control system and to assess its ability to handle off-nominal conditions, the evaluation included 4-g windup turns. These maneuvers were marginally within the scope of this study, owing to the aerodynamic data at angles of attack above 7° to 10° being somewhat questionable. These turns were generally considered to be unsatisfactory with Cooper-Harper ratings ranging from 4 to 10. In most cases, these turns could not be controlled due to differential stabilizer and rudder control surface saturation. This was an extreme task for the OWRA, since the design limit load factor for the airplane will be 4 g.

Windup turns to 3 and 3.5 g could be achieved with high pilot workload and ratings ranging from 4 to 8 (level 2 to 3 handling qualities). As with other tasks, flight condition 1 was the best and flight conditions 4 and 5 were the worst. The pilots commented that the lateral acceleration or sideforce increased markedly as g was increased.

Generally, the pilot comments and ratings deteriorated with both increasing wing skew and dynamic pressure. The most favorable comments and ratings were given for the flight condition with lowest wing skew angle which was also at the lowest dynamic pressure (flight condition 1). The highest dynamic pressure cases with wing skew of 65° received the most unfa-

vorable comments and ratings (flight conditions 4 and 5). Each of the flight conditions contained elements of the unfavorable characteristics to varying degrees. A detailed discussion of flight conditions 1 and 4 follows. These conditions were chosen as being representative of the best and the worst flight conditions, respectively.

Flight Condition 1 ($M = 0.8, h = 20,000$ ft, $\Lambda = 45°$)

In general flight condition 1 was the best flight condition flown, and few adverse comments were received. Overall, the small, intermediate, and large maneuvers (excluding the windup turns to 4 g) were considered to be satisfactory with Cooper-Harper ratings of 2 and 3, level 1 flying qualities. The problems included pitch axis which was described as "too abrupt" or "too much pitch rate overshoot." In addition, some pitch-to-roll and pitch-to-sideforce coupling was evident in the response to pitch inputs. A time response of the longitudinal and lateral-directional data of small pilot commanded pitch pulses for flight condition 1 is presented in figure 9. From this figure it can be seen that the pulses between $t = 60$ sec and 90 sec produced relatively sharp responses in all the longitudinal variables and normal acceleration. Particularly evident is the overshoot in both pitch attitude and pitch rate after the pulse is released. The minor pitch-to-roll and pitch-to-sideforce coupling can be seen in the traces of roll angular rate and lateral acceleration, respectively. Although lateral stick and rudder pedal inputs (not shown) were minimal, these traces show considerable low-level activity resulting from the pitch commands.

It was generally felt that the precision needle tracking tasks presented moderate difficulty and were given pilot ratings from 3 to 5. The air-to-air refueling (station keeping) task was generally satisfactory while the distance from the drogue to the receiver was moderate. At distances approaching that required for hookup, however, maintaining a steady position was extremely difficult, and none of the pilots felt that a hookup could be achieved.

Flight Condition 4 ($M = 1.6, h = 29,000$ ft, $\Lambda = 65°$)

In general flight condition 4 was the worst flight condition flown. Large precision maneuvers displayed objectionable characteristics resulting in Cooper-Harper pilot ratings ranging from 5 to 7. The primary objections were the pitch-to-lateral acceleration and pitch-to-roll coupling. Even though the coupling resulted in objectionable responses, the intermediate maneuvers, when carried out gently, were generally given a Cooper-Harper rating of 3. Aggressive pitch command inputs were not comfortable and were avoided.

One pilot indicated that the airplane seemed to dig in above 3 g (for turns to the left). For the 2-g windup turns, left turns received a pilot rating of 7 while right turns received a pilot rating of 5. Another pilot indicated that if a pull-up was required while banking left, the result was more bank angle which was uncomfortable. In a left turn, as back pressure was increased on the stick, the airplane tended to roll into the bank angle or turn, while in a turn to the right, it tended to roll out of the bank angle. Both of these characteristics were objectionable. Generally the pilots thought that turn coordination was best achieved by keeping their feet off the rudder pedals, and that the airplane was self-coordinating at moderate g levels, while at higher g the airplane was impossible to coordinate. Why the airplane behaved in this manner is discussed in the next section.

The precision needle tracking tasks were rated from 4 to 6 with the pitch-to-sideforce coupling being the most annoying feature. Air-to-air station keeping was accomplished with considerable difficulty.

Aerodynamic and Inertial Coupling

Oblique-wing airplanes display both inertial and aerodynamic coupling. This coupling is a function of Mach number, angle of attack, and wing skew. As expected, some of the OWRA coupling characteristics were found to be similar to the coupling characteristics of the AD-1 airplane (Sim and Curry, 1985). The significant coupling problems in the OWRA are from pitch to roll and pitch to sideforce. Coupling from roll to pitch was minor. All conditions in the VMS were flown with a closed loop flight control system that provided significant decoupling.

Pitch-to-roll coupling

Pitch-to-roll coupling in the open loop configuration was substantial and was a major factor in the design of the closed loop control system. With the

loops closed, only minor pitch-to-roll coupling was reported by the pilots. This roll coupling caused minor handling qualities problems in the VMS tests and was commented on the most in the low dynamic pressure cases. An example of pitch pulses, where minor roll coupling was commented on, is shown for flight condition 1 in figure 9. Where there were no lateral inputs, it can be seen that the roll rates are not generally more than 5°/sec resulting in 4° to 5° of change in bank angle. The lateral acceleration was generally less than 0.2 g. One pilot indicated that the response was similar to a helicopter in that when he pitched up, the airplane rolled right, and when he pitched down, the airplane rolled left.

Pitch-to-sideforce coupling

The pilots participating in the evaluation were unanimous in their complaint that the high level of sideforce or lateral acceleration encountered when performing pitch maneuver tasks was unacceptable. This was particularly pronounced when abrupt pitch maneuvers were required, as in the pitch tracking task. Excessive lateral acceleration was encountered at each of the flight conditions flown except in the low dynamic pressure cases, where pitch-to-sideforce coupling was least objectionable. The most severe problems— rated as unacceptable—occurred at the high dynamic pressure cases (flight conditions 4 and 5). One pilot described as "scary" the large lateral responses as he pulled into a climb and pushed over when evaluating flight condition 5. This led him to rate the airplane unacceptable and he gave it a Cooper-Harper rating of 7. At best, this coupling was rated acceptable but annoying, at the lowest dynamic pressure case (flight condition 1).

Open loop dynamics

A 4-sec time response of the nonlinear dynamics of the open loop and closed loop airplane to a nose up normal acceleration step command of slightly less than 2 g for flight conditions 1 and 4 is shown in figure 10. Flight condition 1 was the lowest dynamic pressure ($\bar{q}$ = 436 lb/ft^2) condition tested while condition 4 was the highest ($\bar{q}$ = 1181 lb/ft^2). These flight conditions received, respectively, the best and worst pilot ratings and comments relative to the lateral acceleration induced in pitch maneuvers.

First, consider the open loop responses. From these responses, it is evident that although the command was purely pitch, there was significant coupling to the lateral-directional axes. This coupling is particularly significant in the roll rate, bank angle, lateral acceleration, and, for flight condition 4, sideslip angle. In flight condition 1, the vehicle rolled to 85° right bank with a change in angle of attack of 2.2°. While in flight condition 4, it rolled almost 360° left with a change in angle of attack of 3.9°. The resulting peak lateral acceleration for condition 1 was approximately -0.2 g while for condition 4 it was -1.25 g.

The primary open loop dynamic behavior of these two flight conditions can be explained as follows. The two major aerodynamic contributors to the roll were (1) the change in rolling moment due to change in angle-of-attack derivative (L_α) and (2) the effective dihedral derivative (L_β). The two major aerodynamic contributors to lateral acceleration were (1) the change in sideforce due to the change in angle-of-attack derivative (Y_α), and (2) the sideforce derivative (Y_β). Each of these derivatives is a nonlinear function of angle of attack, but for the following discussion the linearized derivatives will be considered. The important linearized dimensional aerodynamic derivatives are presented for comparison in table 8. The complete linear models for all flight conditions are presented in appendix C.

Relative magnitudes of L_α and L_β are quite large due to the relatively small value of roll inertia. Note that for flight condition 4, the effective dihedral is particularly large. In flight condition 1, the positive L_α dominates the response with a right roll for a positive change in angle of attack. Relatively small positive values of sideslip angle were generated; therefore, comparatively little sideforce or bank angle due to sideslip was generated. In flight condition 4, the L_α derivative is still positive but the resultant roll was to the left. In this case the generated sideslip angle was also positive or nose left, but larger in magnitude because the larger change in yawing moment due to change in angle-of-attack derivative (N_α), and, therefore, the larger L_β, dominated the response with a roll to the left overpowering the L_α derivative. The sideforce in each flight condition was to the left, and with both the angle of attack and angle of sideslip in phase, the effects of Y_α and Y_β were additive.

Sim and Curry (1985) point out that with increasing angle of attack, the resultant aerodynamic forces on a wing rotate and become approximately perpendicular to the wing sweep angle. For a skewed wing, this results in a large sideforce component. For static trim (to maintain a constant heading), this sideforce must be balanced using either sideslip angle, bank angle, or a combination of sideslip and bank angle. In other words, at skew angles other than zero, if a zero bank angle trim is required, then some steady sideslip will be required. The problem is shown in figure 11 which presents the wind-tunnel sideforce coefficient data for flight conditions 1 and 5. The 1-g trim angles of attack are 1.6° and 1.9°, respectively. The angles of attack of interest range between −2° and 5°. As angle of attack varies, a significant change occurs in sideforce coefficient for both flight conditions, and for condition 1, the variation is even more significant.

Closed loop dynamics

The roll due to angle-of-attack change was virtually eliminated, and the lateral acceleration response was significantly reduced by the control system for both flight conditions as indicated by the closed loop responses (fig. 10). The change in sideslip angle, for both flight conditions, was negative or nose right. With this combination of angle-of-attack and angle-of-sideslip change, the effects of Y_α and Y_β tended to cancel each other and improve the response. The closed loop peak lateral acceleration in flight condition 1 was −0.07 g, while for flight condition 4 it was −0.36 g or a reduction of 65 and 71 percent, respectively, from open loop. Even though the control law significantly reduced peak lateral acceleration, the reduced amplitudes were objectionable to the pilots when performing aggressive pitch maneuvers.

An example of the closed loop pitch tracking task done during a VMS evaluation of flight condition 5 is shown in figure 12. This time response presents a 120-sec interval of the longitudinal and lateral-directional response parameters. From the longitudinal response, it can be seen that there is a high level of pitch activity as the pilot attempts to fly the task. The lateral-directional time response shows that the pilot activity on the lateral stick is minimal until the last 30 sec when the pitch task is combined with a roll task. Observe that during the pitch portion of the task, the lateral acceleration is substantial and in some places is about 0.6 g peak-to-peak amplitude. Angle of attack, lateral acceleration, and sideslip angle, during a portion of this time interval when the pilot's lateral command inputs were very small, are shown in figure 13. From this it appears that for the closed loop configurations, the lateral acceleration is a strong function of angle of attack and not sideslip angle. Thus, it appears that the pitch-to-sideforce coupling was caused by the change in sideforce due to change in angle-of-attack derivative (Y_α) and was the primary source of the lateral acceleration encountered in abrupt pitch maneuvers. This large lateral acceleration resulting from pitch inputs made the airplane unacceptable at high dynamic pressures and annoying at lower dynamic pressures.

Coupling in left and right turns

For flight condition 4, a 2-g left turn received a pilot rating of 7, while a right turn received a rating of 5. This difference was caused by the airplane's tendency to roll into the left bank and out of the right bank. Pilot comments and ratings clearly indicated that they preferred to be rolled out of the turns rather than into the turns. However, neither was considered comfortable. Both the asymmetric response and the uncomfortable feel of the turns combined to make this coupling characteristic clearly unsatisfactory.

This maneuver calls attention to the basic asymmetry of the OWRA. The nonlinear aerodynamic coefficients of rolling moment, yawing moment, and sideforce as a function of angle of attack are presented in figure 14 for flight condition 4. If the airplane were symmetric, these coefficients would be zero and insensitive to changes in angle of attack. Instead they are strong nonlinear functions of angle of attack. As a pilot rolled into either a left or right turn, the angle of attack was increased to maintain altitude. At this flight condition the airplane trims at about 2° angle of attack at 1 g, and at about 4.5° at 2 g. Note the changes in these coefficients as the angle of attack increases from 2° to 4.5° . The positive rolling moment nearly triples yielding a right roll acceleration. The negative yawing moment nearly doubles resulting in a nose left yaw acceleration. Finally the negative sideforce coefficient more than triples giving a left acceleration. These accelerations, being functions of angle of attack, act in the same direction regardless of the direction of the turn. From the curves of figure 14, it is clear that the tendency only gets worse as angle of attack contin-

ues to increase. The trim angle of attack at 3.5 g is 8° . This explains the pilot comment on the 4-g turns that the lateral acceleration increased markedly as the g was increased.

The control law, in general, had sufficient differential stabilizer authority and was able to cope with the roll axis in all but the highest g turns. In all turns, left or right, excessive amounts of right rudder were carried, and at higher g levels, the rudder surface reached its position limit. This trend was fairly typical of all flight conditions and was related to the same coupling characteristics in the pitch axis. At flight conditions 4 and 5, the dynamic behavior of the airplane was aggravated by the high dynamic pressure.

In prior fixed-base simulation at Ames-Dryden, there were no pilot comments concerning either the pitch-to-sideforce coupling, or the asymmetry of the turns. The fixed-base simulator did not have a visual display, and so the pilots flew entirely by using instruments. The cockpit did contain a complete set of instruments including a lateral accelerometer. Even though in typical pitch and roll maneuvers the lateral accelerations were significant, the pilots did not seem to object to this coupling. It is concluded that the lack of both motion and visual cues resulted in the pilot's acceptance of this unusual coupling. The only adverse comments in the fixed-base operation were related to the relatively minor pitch-to-roll coupling.

From the foregoing discussion, it appears that for the closed loop configurations, the pitch-to-sideforce coupling through the change in sideforce due to change in angle-of-attack derivative (Y_α) was the primary source of the pilot's lateral acceleration in abrupt pitch maneuvers. This lateral acceleration rendered the airplane unacceptable at high dynamic pressure and annoying at lower dynamic pressure. The control system, while providing satisfactory pitch-to-roll decoupling at all flight conditions, did not provide acceptable pitch-to-sideforce decoupling. The asymmetrical coupling in turns was related to the variation of rolling and yawing moments and sideforce as a function of angle of attack which are a direct function of the asymmetric nature of the configuration. Both of these characteristics were objectionable to the pilots. This unusual coupling was objectionable with a motion-base simulator; in a fixed-base simulator, the pilots only objected to the minor pitch-to-roll coupling. The use of a motion-base simulation with visual cues provided conclusions about handling qualities for this vehicle that were not obvious using a fixed-base simulation with no visual cues.

Effect of Cockpit Side Acceleration on Pilot Rating

The preceding sections dealt with the general handling qualities of the OWRA with control laws based on loopshaping and with the major coupling characteristics that (1) had to be considered in control law design, and (2) were still evident after the control loops were closed. The most troublesome of these characteristics was residual side acceleration at the cockpit in response to pitch control inputs.

Vertical motion simulation comparison

Figure 15 shows cockpit side acceleration and normal acceleration responses to aft stick step inputs for flight conditions 1 and 4. Both the accelerations computed for the airplane (output of the simulation math model) and those generated as commands to the simulator (outputs of the VMS motion washout program) are presented. The effects of the motion washouts are clearly shown. The degree of attenuation of normal acceleration change Δa_{nP} was much greater than that of side acceleration a_{yP} because of the greater magnitude of Δa_{nP} computed for the airplane and because of the lack of additional means to generate long-term acceleration cues (other than 1 g). In the case of longitudinal or side acceleration, cab tilt is introduced so that these cues approach the steady-state values computed for the vehicle.

Variation of pilot rating with side acceleration

Even though the present study is preliminary, it is desirable to quantify the results that may be of use as design criteria. At present, no criteria exist that set limits on side acceleration response during longitudinal maneuvers, simply because they are not of concern in conventional aircraft (with the possible exception of helicopters).

In looking for a parameter to express the disturbing effects of side acceleration on the pilot, several alternatives were considered, based on ratios of accelerations (for example, lateral, normal, simulator cab, or computed for the flight vehicle). Of these, the parameter selected was one that related peak a_{yP} command to the VMS cab (a close approximation to the actual

cab acceleration) to the steady-state change in normal acceleration $\Delta a_{nP,ss}$ computed for the flight vehicle, in response to a nose-up step input at the stick. The resulting side-acceleration parameter is

$$A(y/n) = \left| \frac{a_{yP,max}(\text{VMS})}{\Delta a_{nP,ss}(\text{OWRA})} \right|$$

The denominator $\Delta a_{nP,ss}(\text{OWRA})$ was chosen in preference to normal acceleration command to the VMS because it was considered a better measure of expected airplane maneuvering level. Values of the side-acceleration parameter for the five flight conditions, measured from responses similar to those of figure 15, are shown in table 9. Average and root mean square (RMS) overall pilot ratings for each case are included.

These data, as well as the individual pilot ratings, are plotted in figure 16. The shaded band through the average ratings is equal in width to twice the average RMS pilot rating.

Although other handling qualities factors were included in arriving at an overall rating by the pilots, these results show a clear degradation with increasing side-acceleration disturbance. At a value of the side-acceleration parameter of approximately 0.3, objectionable to major deficiencies (PR = 6.5) should be expected, requiring improvement. Taking into account the effects of the VMS motion washout, it is noted that the pilot would experience even greater sideforce disturbances in the actual OWRA flight demonstrator, underscoring the need for further control law development. For future application of an oblique wing to service aircraft, the addition of independent sideforce-generating surfaces might be considered.

All preceding results must be viewed in perspective. The OWRA VMS evaluation was carried out on a preliminary control law for a preliminary flight configuration. It was proposed to increase the wing area of the OWRA to 300 ft^2 and to mount the wing at a 10° right wing down cant angle (at $\Lambda = 65°$), with respect to the fuselage, to alleviate the asymmetric sideforce, yawing, and rolling moments. Early indications are that the increased wing area and cant angle would tend to alleviate some of the severe aerodynamic coupling problems. However, the OWRA would be a demonstrator airplane with an existing fuselage and empennage and not an optimized oblique-wing airplane configuration.

CONCLUDING REMARKS

A large vertical motion piloted simulation of an early version of the F-8 oblique wing research airplane was conducted to assess the performance of a preliminary decoupling control law. A total of six pilots participated in the evaluation of five discrete flight conditions. Various maneuvers were evaluated at each of the flight conditions for which the pilots gave written comments and numerical ratings. From this simulation and analysis of the data, the following conclusions were drawn:

1. Participating pilots were unanimous that the high levels of sideforce or lateral acceleration in pitch maneuvers were unsatisfactory.

2. Pilots were more critical of left turns than they were of right turns. At the higher dynamic pressure conditions, the difference was as much as 2 pilot ratings. Pilots indicated that the airplane rolled into the bank angle in left turns and rolled out of the bank angle in right turns.

3. Pilot comments and ratings deteriorated with both increasing wing skew and dynamic pressure. The most favorable comments were received for the lowest dynamic pressure and wing skew condition, and the most unfavorable comments were received for the highest dynamic pressure and wing skew condition.

4. Roll-to-pitch coupling was not a significant problem.

5. Pitch-to-roll coupling in the open loop configuration was substantial and was a major concern in the control law design. This coupling caused only minor handling qualities problems in the closed loop airplane.

6. The flight control system provided satisfactory pitch-to-roll decoupling at all flight conditions, but did not provide acceptable pitch-to-sideforce decoupling.

7. The use of a motion-base simulation with visual cues provided handling qualities conclusions for

this vehicle that were not obvious using a fixed-base simulation with no visual cues.

Ames Research Center
Dryden Flight Research Facility
National Aeronautics and Space Administration
Edwards, California, March 9, 1988

APPENDIX A—F-8 OWRA CENTER OF GRAVITY AND MASS DISTRIBUTION

Weight with 50 percent fuel = 21,116 lb
Reference center of gravity XREF = 454.00 in.
YREF = 0
ZREF = 100.00 in.

Wing skew, deg	0	45	55	65
$\Delta X \sim$ ft (from ref. c.g.)	0.325	0.334	0.328	0.343
$\Delta Y \sim$ ft	0	0.022	0.026	0.029
$\Delta Z \sim$ ft	−0.546	−0.546	−0.544	−0.546
$I_{xx} \sim$ slug-ft^2	12,084.6	8,218.3	6910.8	5,733.0
$I_{yy} \sim$ slug-ft^2	89,251.8	93,120.5	94,569.6	95,608.0
$I_{zz} \sim$ slug-ft^2	95,590.7	95,592.8	95,718.9	95,595.2
$I_{xz} \sim$ slug-ft^2	2,932.1	2,911.1	2,897.6	2,892.2
$I_{xy} \sim$ slug-ft^2	0	3,869.1	3,636.6	2,965.4
$I_{yz} \sim$ slug-ft^2	0	−29.0	−56.6	−62.6

APPENDIX B— CONTROL LAW GAINS AND FILTER VARIABLES USED IN THE VMS STUDY

(a) Variables as a function of flight condition

Variable	Flight condition 1	Flight condition 2	Flight condition 3	Flight condition 4	Flight condition 5
h rad/sec	97	150	182	210	128
f rad/sec	4.2	6.3	7.8	9.5	8.3
H_1	23	21	15	10	14
p_1 rad/sec	2.5	3.3	3.3	3.4	4.5
H_2	3.0	8.3	3.0	5.6	30
p_2 rad/sec	10	1.1	10	1.0	10
K_{11} sec	0.0490	0.0220	0.0200	0.0150	0.0130
K_{21} sec	0.0120	0.0045	0.0074	−0.0013	0.0032
K_{31} sec	0.0024	0.0012	0.0014	0.00098	0.00059
K_{12} rad/g	0.0039	0.0021	0.0015	0.0010	0.0013
K_{22} rad/g	−0.0049	−0.0051	−0.0050	−0.0045	−0.0016
K_{32} rad/g	$-5.3(10)^{-6}$	$-1.3(10)^{-6}$	$-6.6(10)^{-6}$	$-8.4(10)^{-7}$	$-4.5(10)^{-7}$
K_{13} rad/g	−0.0019	−0.00084	−0.00089	−0.00065	−0.00054
K_{23} rad/g	−0.00046	−0.00048	−0.00027	$-2.6(10)^{-5}$	−0.00016
K_{33} rad/g	−0.0046	−0.0031	−0.0028	−0.0025	−0.0015
H_{11}	0.1500	0.0310	0.0490	0.0270	0.0360
H_{21}	0.0400	0.0180	0.0280	0.0130	0.0170
H_{31}	0.0170	0.0048	0.0110	0.0053	0.0056
H_{12} rad/sec/g	0.0055	0.0046	0.0028	0.0019	0.0025
H_{22} rad/sec/g	−0.0140	−0.0170	−0.0160	−0.0140	−0.0074
H_{32} rad/sec/g	$-5.7(10)^{-5}$	$-1.9(10)^{-5}$	$-5.4(10)^{-5}$	$-1.4(10)^{-5}$	$-6.4(10)^{-6}$
H_{13} rad/sec/g	−0.0120	−0.0019	−0.0047	−0.0020	−0.0028
H_{23} rad/sec/g	−0.0025	−0.0005	−0.00072	−0.00048	−0.00063
H_{33} rad/sec/g	−0.0045	−0.0033	−0.0038	−0.0032	−0.0040

(b) Variables constant with flight condition

i	a_i rad/sec	c_i	b_i rad/sec
1	20.0	0.33	18.75
2	20.0	0.33	18.75
3	20.0	0.50	56.6
4	20.0	1.0	37.7
5	20.0	1.0	37.7

APPENDIX C—LINEARIZED STATE SPACE MODELS

The linearized state space models for each of the five flight conditions used in development of the control law are presented in this appendix. These models are for a 200 ft^2 wing preliminary aerodynamic data base and are referenced to vehicle body axes at 1-g trim. The matrices are of the following format:

$$C\dot{x} = Ax + Bu$$

where the state vector is

$$x = \begin{bmatrix} V \\ \alpha \\ \beta \\ \phi \\ \theta \\ p \\ q \\ r \end{bmatrix}$$

and the control vector is

$$u = \begin{bmatrix} \delta_{eL} \\ \delta_{eR} \\ \delta_{aL} \\ \delta_{aR} \\ \delta_r \end{bmatrix}$$

Flight condition 1

A matrix

$$\begin{bmatrix} -0.0110 & 23.2260 & 11.0221 & -0.1557 & -32.1120 & 0.0067 & -0.0006 & -0.0309 \\ -0.0001 & -0.8219 & 0.1018 & 0.0000 & 0.0000 & 0.0037 & 0.9926 & -0.0002 \\ 0.0000 & -0.0677 & -0.2915 & 0.0387 & -0.0002 & 0.0321 & 0.0001 & -0.9918 \\ 0.0000 & 0.0000 & 0.0000 & 0.0000 & 0.0000 & 1.0000 & 0.0000 & 0.0337 \\ 0.0000 & 0.0000 & 0.0000 & 0.0000 & 0.0000 & 0.0000 & 1.0000 & 0.0000 \\ 0.0003 & 41.5817 & -54.7588 & 0.0000 & 0.0000 & -3.2018 & 2.5429 & 1.8897 \\ -0.0000 & -10.4093 & 3.0050 & 0.0000 & 0.0000 & 0.2980 & -1.1222 & 0.1127 \\ -0.0005 & -2.1243 & 12.3733 & 0.0000 & 0.0000 & 0.0739 & -0.0583 & -0.7666 \end{bmatrix}$$

B matrix

$$\begin{bmatrix} 2.9838 & -4.5317 & -1.1352 & -0.8126 & 3.6380 \\ -0.0967 & -0.0967 & -0.0185 & -0.0289 & 0.0000 \\ -0.0167 & 0.0167 & 0.0015 & -0.0010 & 0.0649 \\ 0.0000 & 0.0000 & 0.0000 & 0.0000 & 0.0000 \\ 0.0000 & 0.0000 & 0.0000 & 0.0000 & 0.0000 \\ 16.6821 & -16.3952 & 13.6724 & -12.1893 & 15.2320 \\ -9.9451 & -9.9741 & -1.5331 & 1.2841 & 0.0153 \\ 1.5915 & -1.5909 & -0.0234 & -0.0592 & -6.6653 \end{bmatrix}$$

C matrix

$$\begin{bmatrix} 1.0000 & 0.0000 & 0.0000 & 0.0000 & 0.0000 & 0.0000 & 0.0000 & 0.0000 \\ 0.0000 & 1.0000 & 0.0000 & 0.0000 & 0.0000 & 0.0000 & 0.0000 & 0.0000 \\ 0.0000 & 0.0000 & 1.0000 & 0.0000 & 0.0000 & 0.0000 & 0.0000 & 0.0000 \\ 0.0000 & 0.0000 & 0.0000 & 1.0000 & 0.0000 & 0.0000 & 0.0000 & 0.0000 \\ 0.0000 & 0.0000 & 0.0000 & 0.0000 & 1.0000 & 0.0000 & 0.0000 & 0.0000 \\ 0.0000 & 0.0000 & 0.0000 & 0.0000 & 0.0000 & 1.0000 & -0.4708 & -0.3543 \\ 0.0000 & 0.0000 & 0.0000 & 0.0000 & 0.0000 & -0.0415 & 1.0000 & 0.0005 \\ 0.0000 & 0.0000 & 0.0000 & 0.0000 & 0.0000 & -0.0305 & 0.0005 & 1.0000 \end{bmatrix}$$

Flight condition 2

A matrix

$$\begin{bmatrix} -0.0233 & 10.8460 & 17.0214 & -0.5940 & -32.0786 & 0.0276 & -0.0018 & -0.1415 \\ 0.0000 & -0.5463 & 0.0755 & 0.0000 & 0.0000 & 0.0183 & 0.9939 & 0.0008 \\ 0.0000 & -0.0665 & -0.3772 & 0.0267 & -0.0005 & 0.0587 & 0.0001 & -0.9918 \\ 0.0000 & 0.0000 & 0.0000 & 0.0000 & 0.0000 & 1.0000 & 0.0000 & 0.0601 \\ 0.0000 & 0.0000 & 0.0000 & 0.0000 & 0.0000 & 0.0000 & 1.0000 & 0.0000 \\ 0.0061 & 33.4361 & -153.2500 & 0.0000 & 0.0000 & -1.7801 & 0.9704 & 2.6802 \\ 0.0004 & -24.8222 & 6.2928 & 0.0000 & 0.0000 & 0.1250 & -1.1551 & 0.1386 \\ -0.0013 & -4.2295 & 21.8795 & 0.0000 & 0.0000 & 0.1276 & -0.0930 & -1.0235 \end{bmatrix}$$

B matrix

$$\begin{bmatrix} -0.5349 & -12.1382 & -0.5669 & -0.8690 & 5.2017 \\ -0.0788 & -0.0788 & -0.0042 & -0.0076 & 0.0000 \\ -0.0149 & -0.0147 & -0.0006 & -0.0005 & 0.0254 \\ 0.0000 & 0.0000 & 0.0000 & 0.0000 & 0.0000 \\ 0.0000 & 0.0000 & 0.0000 & 0.0000 & 0.0000 \\ 41.6268 & -41.0035 & 5.3175 & -4.7375 & 17.2967 \\ -13.6669 & -13.7094 & -0.6941 & 0.9921 & 0.0224 \\ 2.3819 & -2.3821 & -0.0150 & -0.0775 & -4.2803 \end{bmatrix}$$

C matrix

$$\begin{bmatrix} 1.0000 & 0.0000 & 0.0000 & 0.0000 & 0.0000 & 0.0000 & 0.0000 & 0.0000 \\ 0.0000 & 1.0000 & 0.0000 & 0.0000 & 0.0000 & 0.0000 & 0.0000 & 0.0000 \\ 0.0000 & 0.0000 & 1.0000 & 0.0000 & 0.0000 & 0.0000 & 0.0000 & 0.0000 \\ 0.0000 & 0.0000 & 0.0000 & 1.0000 & 0.0000 & 0.0000 & 0.0000 & 0.0000 \\ 0.0000 & 0.0000 & 0.0000 & 0.0000 & 1.0000 & 0.0000 & 0.0000 & 0.0000 \\ 0.0000 & 0.0000 & 0.0000 & 0.0000 & 0.0000 & 1.0000 & -0.5172 & -0.5045 \\ 0.0000 & 0.0000 & 0.0000 & 0.0000 & 0.0000 & -0.0310 & 1.0000 & 0.0007 \\ 0.0000 & 0.0000 & 0.0000 & 0.0000 & 0.0000 & -0.0303 & 0.0007 & 1.0000 \end{bmatrix}$$

Flight condition 3
A matrix

$$\begin{bmatrix} -0.0282 & 3.4110 & 21.3483 & 0.0976 & -32.0839 & -0.0050 & 0.0001 & 0.0236 \\ 0.0000 & -0.8756 & 0.0746 & 0.0000 & 0.0000 & -0.0042 & 0.9962 & -0.0005 \\ 0.0000 & -0.0264 & -0.4223 & 0.0229 & 0.0001 & 0.0217 & 0.0000 & -0.9942 \\ 0.0000 & 0.0000 & 0.0000 & 0.0000 & 0.0000 & 1.0000 & 0.0000 & 0.0229 \\ 0.0000 & 0.0000 & 0.0000 & 0.0000 & 0.0000 & 0.0000 & 1.0000 & 0.0000 \\ -0.0024 & 102.4630 & -148.3910 & 0.0000 & 0.0000 & -2.7802 & 2.2394 & 2.9470 \\ 0.0022 & -21.9861 & 10.6326 & 0.0000 & 0.0000 & 0.3038 & -1.4218 & 0.1912 \\ -0.0009 & -14.1234 & 25.2211 & 0.0000 & 0.0000 & 0.0871 & -0.0808 & -1.0807 \end{bmatrix}$$

B matrix

$$\begin{bmatrix} -21.1203 & -4.7654 & -0.5126 & -1.2742 & 7.1964 \\ -0.0591 & -0.0591 & -0.0107 & -0.0204 & 0.0000 \\ -0.0036 & 0.0036 & -0.0003 & 0.0008 & 0.0211 \\ 0.0000 & 0.0000 & 0.0000 & 0.0000 & 0.0000 \\ 0.0000 & 0.0000 & 0.0000 & 0.0000 & 0.0000 \\ 43.9185 & -43.5091 & 13.5081 & -17.0883 & 13.8560 \\ -13.7467 & -13.6839 & -1.4792 & 1.8304 & 0.0274 \\ 1.2327 & -1.2366 & 0.0308 & -0.1561 & -4.2793 \end{bmatrix}$$

C matrix

$$\begin{bmatrix} 1.0000 & 0.0000 & 0.0000 & 0.0000 & 0.0000 & 0.0000 & 0.0000 & 0.0000 \\ 0.0000 & 1.0000 & 0.0000 & 0.0000 & 0.0000 & 0.0000 & 0.0000 & 0.0000 \\ 0.0000 & 0.0000 & 1.0000 & 0.0000 & 0.0000 & 0.0000 & 0.0000 & 0.0000 \\ 0.0000 & 0.0000 & 0.0000 & 1.0000 & 0.0000 & 0.0000 & 0.0000 & 0.0000 \\ 0.0000 & 0.0000 & 0.0000 & 0.0000 & 1.0000 & 0.0000 & 0.0000 & 0.0000 \\ 0.0000 & 0.0000 & 0.0000 & 0.0000 & 0.0000 & 1.0000 & -0.5273 & -0.4209 \\ 0.0000 & 0.0000 & 0.0000 & 0.0000 & 0.0000 & -0.0385 & 1.0000 & 0.0006 \\ 0.0000 & 0.0000 & 0.0000 & 0.0000 & 0.0000 & -0.0304 & 0.0006 & 1.0000 \end{bmatrix}$$

Flight condition 4
A matrix

$$\begin{bmatrix} -0.0166 & 0.4263 & 16.2201 & -0.2355 & -32.0832 & 0.0127 & -0.0003 & -0.0605 \\ 0.0000 & -0.6332 & 0.0733 & 0.0000 & 0.0000 & 0.0069 & 0.9959 & -0.0001 \\ 0.0000 & -0.0591 & -0.5031 & 0.0201 & -0.0001 & 0.0313 & 0.0000 & -0.9943 \\ 0.0000 & 0.0000 & 0.0000 & 0.0000 & 0.0000 & 1.0000 & 0.0000 & 0.0324 \\ 0.0000 & 0.0000 & 0.0000 & 0.0000 & 0.0000 & 0.0000 & 1.0000 & 0.0000 \\ 0.0026 & 82.4155 & -278.6200 & 0.0000 & 0.0000 & -2.0724 & 1.1343 & 3.3002 \\ 0.0004 & -25.1980 & 13.1075 & 0.0000 & 0.0000 & 0.1684 & -1.3592 & 0.1883 \\ -0.0006 & -16.0413 & 26.2952 & 0.0000 & 0.0000 & 0.1203 & -0.0584 & -1.1472 \end{bmatrix}$$

B matrix

$$\begin{bmatrix} 9.0822 & -12.3679 & -0.4790 & -0.8880 & 9.0606 \\ -0.1510 & -0.1510 & -0.0032 & -0.0123 & 0.0000 \\ 0.0013 & -0.0013 & -0.0013 & -0.0020 & 0.0189 \\ 0.0000 & 0.0000 & 0.0000 & 0.0000 & 0.0000 \\ 0.0000 & 0.0000 & 0.0000 & 0.0000 & 0.0000 \\ 68.9285 & -67.3396 & 7.1377 & -8.7943 & 16.2479 \\ -16.3865 & -16.4685 & -0.7968 & 1.6846 & 0.0355 \\ -0.2574 & 0.2598 & -0.2849 & -0.2943 & -4.4829 \end{bmatrix}$$

C matrix

$$\begin{bmatrix} 1.0000 & 0.0000 & 0.0000 & 0.0000 & 0.0000 & 0.0000 & 0.0000 & 0.0000 \\ 0.0000 & 1.0000 & 0.0000 & 0.0000 & 0.0000 & 0.0000 & 0.0000 & 0.0000 \\ 0.0000 & 0.0000 & 1.0000 & 0.0000 & 0.0000 & 0.0000 & 0.0000 & 0.0000 \\ 0.0000 & 0.0000 & 0.0000 & 1.0000 & 0.0000 & 0.0000 & 0.0000 & 0.0000 \\ 0.0000 & 0.0000 & 0.0000 & 0.0000 & 1.0000 & 0.0000 & 0.0000 & 0.0000 \\ 0.0000 & 0.0000 & 0.0000 & 0.0000 & 0.0000 & 1.0000 & -0.5172 & -0.5045 \\ 0.0000 & 0.0000 & 0.0000 & 0.0000 & 0.0000 & -0.0310 & 1.0000 & 0.0007 \\ 0.0000 & 0.0000 & 0.0000 & 0.0000 & 0.0000 & -0.0303 & 0.0007 & 1.0000 \end{bmatrix}$$

Flight condition 5
A matrix

$$\begin{bmatrix} -0.0435 & 9.2212 & 21.3520 & -0.3045 & -32.1705 & 0.0283 & -0.0037 & -0.1486 \\ -0.0001 & -0.9707 & 0.1060 & 0.0000 & 0.0000 & 0.0088 & 0.9852 & -0.0003 \\ 0.0000 & -0.1086 & -0.7545 & 0.0320 & -0.0003 & 0.0357 & 0.0004 & -0.9836 \\ 0.0000 & 0.0000 & 0.0000 & 0.0000 & 0.0000 & 1.0000 & 0.0000 & 0.0388 \\ 0.0000 & 0.0000 & 0.0000 & 0.0000 & 0.0000 & 0.0000 & 1.0000 & 0.0000 \\ 0.0030 & 49.0961 & -233.3070 & 0.0000 & 0.0000 & -3.3659 & 2.2087 & 5.5458 \\ 0.0002 & -37.3890 & 5.6311 & 0.0000 & 0.0000 & 0.2827 & -2.5003 & 0.1287 \\ -0.0018 & -9.0122 & 36.6841 & 0.0000 & 0.0000 & 0.2281 & -0.0090 & -1.9811 \end{bmatrix}$$

B matrix

$$\begin{bmatrix} 6.3985 & -14.0661 & -0.9834 & -0.7068 & 9.4506 \\ -0.2238 & -0.2238 & -0.0192 & -0.0137 & 0.0000 \\ -0.0393 & 0.0393 & -0.0015 & -0.0001 & 0.1146 \\ 0.0000 & 0.0000 & 0.0000 & 0.0000 & 0.0000 \\ 0.0000 & 0.0000 & 0.0000 & 0.0000 & 0.0000 \\ 64.9444 & -63.4666 & 13.1270 & -7.0425 & 55.1392 \\ -27.7743 & -27.8498 & -2.3370 & 1.5383 & 0.0405 \\ 4.8835 & -4.8816 & 0.0128 & -0.1220 & -16.4183 \end{bmatrix}$$

C matrix

$$\begin{bmatrix} 1.0000 & 0.0000 & 0.0000 & 0.0000 & 0.0000 & 0.0000 & 0.0000 & 0.0000 \\ 0.0000 & 1.0000 & 0.0000 & 0.0000 & 0.0000 & 0.0000 & 0.0000 & 0.0000 \\ 0.0000 & 0.0000 & 1.0000 & 0.0000 & 0.0000 & 0.0000 & 0.0000 & 0.0000 \\ 0.0000 & 0.0000 & 0.0000 & 1.0000 & 0.0000 & 0.0000 & 0.0000 & 0.0000 \\ 0.0000 & 0.0000 & 0.0000 & 0.0000 & 1.0000 & 0.0000 & 0.0000 & 0.0000 \\ 0.0000 & 0.0000 & 0.0000 & 0.0000 & 0.0000 & 1.0000 & -0.5172 & -0.5045 \\ 0.0000 & 0.0000 & 0.0000 & 0.0000 & 0.0000 & -0.0310 & 1.0000 & 0.0007 \\ 0.0000 & 0.0000 & 0.0000 & 0.0000 & 0.0000 & -0.0303 & 0.0007 & 1.0000 \end{bmatrix}$$

APPENDIX D—F-8 OWRA, VMS SIMULATION, JANUARY 1987

Pilot Comment Card

Pilot_____ Date_____
Flight condition_____

A. STRAIGHT AND LEVEL; SMALL PILOT DISTURBANCES

1. Frequency and damping characteristics:

   a. Long. inputs _____

   b. Lat./Dir. inputs_____

2. Responses to single-axis inputs (Normal? Objectionable? — Describe):

   a. Pitch stick_____

   b. Roll stick_____

   c. Pedals_____
   Any noticeable coupling (Describe)_____
   Any objectionable coupling (Describe)_____

3. Control forces/harmony_____

B. INTERMEDIATE MANEUVERS

1. Ease of establishing bank angle/turn rate_____

2. Ease of attaining rollout on desired heading_____

3. Ease of establishing new altitude_____

   a. Noticeable/objectionable coupling?_____

4. Ease of executing climbing/descending turns_____

5. Control forces/harmony_____

6. Additional comments_____

C. LARGE MANEUVERS

1. 2-*g* turns (rapid entry and rollout):

   a. Ease of acquiring and maintaining proper bank angle_____
   _____

   b. Ease of maintaining altitude_____

   c. Any objectionable pitch or altitude excursions on entry or rollout_____
   _____
   _____

   d. Turn coordination requirements: Self coordinated?_____
   Excessive pedal required?_____

   e. Pitch/roll control harmony_____

2. Windup turns to 4-*g*

   a. Can altitude be maintained?_____

   b. Turn coordination requirements_____

   c. Pitch stick force per *g*_____

3. Additional comments_____
   _____

D. OVERALL COOPER-HARPER RATING:_____
Major deficiencies, if any_____
_____

E. PRECISION NEEDLE TRACKING TASKS

1. Roll task:
   _____
   Own impression of performance_____

2. Pitch/roll task:
   Difficulty_____
   Own impression of performance_____

F. AIR-TO-AIR REFUELING (STATION KEEPING)

1. Ease of transition to station_____

2. Ease of maintaining station_____

3. Any objectionable characteristics_____

4. Cooper-Harper rating for task_____

REFERENCES

Cooper, G.E. and R.P. Harper, Jr., *The Use of Pilot Rating in the Evaluation of Aircraft Handling Qualities*, NASA TN D-5153, 1969.

Curry, R.E. and A.G. Sim, Unique Flight Characteristics of the AD-1 Oblique-Wing Research Airplane, *AIAA Journal of Aircraft*, vol. 20, no. 6, June 1983, pp. 564–568.

Curry, R.E. and A.G. Sim, *In-Flight Total Forces, Moments, and Static Aeroelastic Characteristics of an Oblique-Wing Research Airplane*, NASA TP-2224, 1984.

Enns, D.F., *Model Reduction for Control System Design*, NASA CR-170417, 1985.

Enns, D.F., D.J. Bugajski, and M.J. Klepl: Flight Control for the F-8 Oblique-Wing Research Aircraft, *Proceedings of the 1987 American Control Conference*, Minneapolis, 1987, p. 1112.

Gregory, Tom, Oblique Wing Ready for Research Aircraft, *Aerospace America.*, June 1985, pp. 78–84.

Holt, D.J., Oblique Wing—New Approach to an Old Problem, *Aerospace Engineering*, vol. 5 Oct. 1985, pp. 26–29.

McFarland, R.E., *Transport Delay Compensation for Computer-Generated Imagery Systems*, NASA TM-100084, 1988.

Meeker, J.I., and G.W. Hall, *In-Flight Evaluation of Lateral-Directional Handling Qualities for the Fighter Mission*, Cornell Aeronautical Laboratory, Inc., Buffalo, New York, AFFDL-TR-67-98, Oct. 1967.

MIL-F-8785C, *Flying Qualities of Piloted Airplanes*, Military Specification, U.S. Air Force, Nov. 1980.

Sim, A.G. and R.E. Curry, *Flight-Determined Aerodynamic Derivatives of the AD-1 Oblique-Wing Research Airplane*, NASA TP-2222, 1984.

Sim, A.G. and R.E. Curry, *Flight Characteristics of the AD-1 Oblique-Wing Research Aircraft*, NASA TP-2223, 1985.

Szalai, K.J., C.R. Jarvis, G.E. Krier, V.A. Megna, L.D. Brock, and R.N. O'Donnell, *Digital Fly-By-Wire Flight Control Validation Experience*, NASA TM-72860, 1978.

TABLE 1. DIMENSIONS AND PHYSICAL CHARACTERISTICS

	F-8 DFBW	OWRA ($\Lambda = 0°$)
Wing area $\sim S$	375 ft^2	200 ft^2
Mean geometric chord $\sim \bar{c}$	11.78 ft	4.78 ft
Wing span $\sim b$	35.67 ft	45.17 ft
Reference center of gravity $\sim X_{REF}$	26.7 percent of $\bar{c}$	44.93 percent of $\bar{c}$
Wing pivot point $\sim X_P$		447.50 in. (33.6 percent of $\bar{c}$)
Aspect ratio $\sim AR$	3.39	10.2
Variable incidence	8°	8°
Fuselage length	52.8 ft	52.8 ft

TABLE 2. VMS MOTION SYSTEM PERFORMANCE CHARACTERISTICS

Mode	Maximum displacement	Maximum velocity	Maximum acceleration	Frequency at 30° phase lag, Hz
Vertical	±25.25 ft	±16 ft/sec	±24 ft/sec^2	0.84
Lateral	±17, −18 ft	±8 ft/sec	±15 ft/sec^2	1.64
Longitudinal	±2.5 ft	±2 ft/sec	±2 ft/sec^2	0.7
Roll angle	±19.5°	±19.5°/sec	±57.3°/sec^2	1.21
Pitch angle	+20, −24.5°	±19.5°/sec	±57.3°/sec^2	1.07
Yaw angle	±34°	±19.5°/sec	±57.3°/sec^2	1.08

TABLE 3 . STICK AND RUDDER PEDAL FORCE CHARACTERISTICS USED IN THE VMS

Control	Breakout, lb	Gradient, lb/in.	Deflection, in.	Hysteresis, lb	Frequency, rad/sec	Damping ratio
Pitch ~ δ_{ES}	1.0	3.5	3.1 forward, 7.0 aft	1.0	14.46	0.32
Roll ~ δ_{LS}	0.75	2.75	±4.0	0.75	14.94	0.21
Rudder ~ δ_{RP}	7.5	27.0	±3.5	5.0	(not available)	

TABLE 4. SURFACE ACTUATOR TRANSFER FUNCTIONS AND SURFACE RATE AND POSITION LIMITS

Surface	Position limit , deg	Rate limit, deg/sec	Actuator transfer function
δ_{eL} and δ_{eR}	+11.75 to −26.5	±25	$18.75/s + 18.75$
δ_r	±17.0*	±78	$56.6/s + 56.6$

*The pilot had the capability of trimming the rudder an additional 4°.

TABLE 5. FLIGHT CONDITIONS INVESTIGATED IN THE VMS STUDY
(Trimmed 1 g initial conditions for $\phi_0 = 0°$)

No.	Mach	h, ft	Λ, deg	$\bar{q}$, lb/ft^2	V_0, ft/sec	V_e, knots	α_0, deg	β_0, deg	δ_{eL}, deg	δ_{eR}, deg	δ_r, deg
1	0.8	20,000	45	436	830	359	1.6	−0.23	−6.3	2.9	−3.4
2	1.2	29,000	65	665	1199	443	3.1	−0.99	−4.1	−1.8	−10.0
3	1.4	29,000	55	905	1399	516	1.4	0.13	1.5	−0.7	−1.1
4	1.6	29,000	65	1181	1599	590	1.8	−0.35	−0.6	0.4	−7.3
5	0.9	500	65	1179	1003	590	1.9	−0.40	−2.8	−0.7	−3.8

TABLE 6. SUMMARY OF OWRA VMS EVALUATION OF PILOT'S EXPERIENCE

Pilot	Total Flight Time, hr	Experience summary
1	3800	Primary experience in high-performance turbojet fighters with a significant amount of time in helicopters
2	10,000	Primary experience in fighter type aircraft with significant multiengine and rotary wing time; over 28 yr of experience
3	9500	Diversified experience in over 100 aircraft types with over 20 yr as a test pilot; significant amount of time in high-performance turbojet fighter aircraft; significant participation in the AD-1 oblique-wing flight test program
4	11,400	Diversified experience in over 84 aircraft types with 29 yr experience; 5700 hr in fighter aircraft and 5300 hr in large multiengine aircraft and the space shuttle
5	2300	Primary experience in a high-performance A-7 attack aircraft; graduate of a recognized test pilot school
6	2300	Primary experience in F-4 and F-14 high-performance fighter aircraft; graduate of a recognized test pilot school

TABLE 7. PILOT RATING SCALE

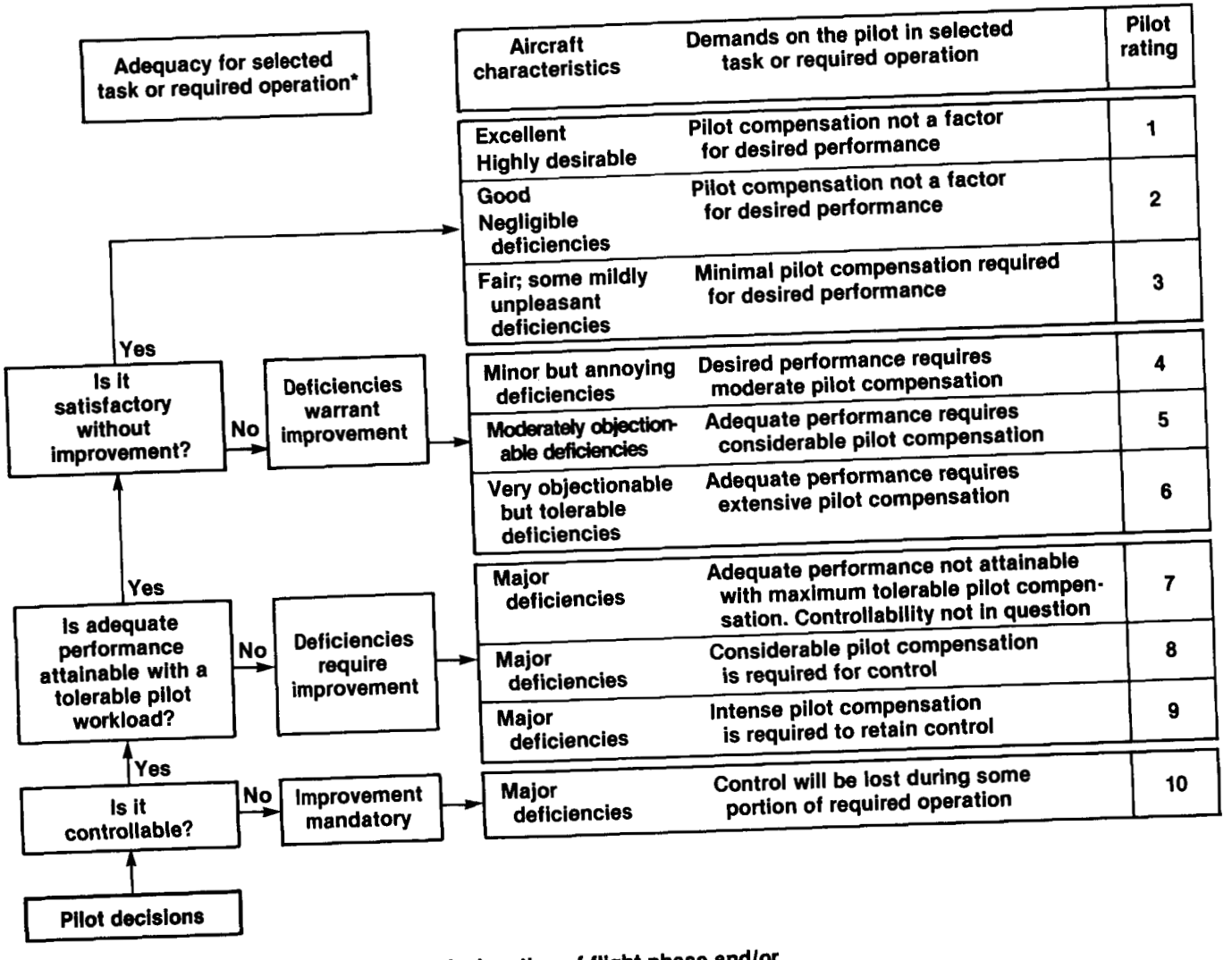

* Definition of required operation involves designation of flight phase and/or subphases with accompanying conditions

8343

TABLE 8. LINEARIZED DIMENSIONAL AERODYNAMIC DERAVITIVES FOR 1-g FLIGHT

	Flight condition	
Derivative	1	4
L_α	41.6	82.4
L_β	−54.8	−278.6
N_α	−2.1	−16.0
Y_α	−0.0677	−0.0591
Y_β	−0.2915	−0.5031

TABLE 9. SIDE ACCELERATION PARAMETER AND AVERAGE PILOT RATING DATA

Flt. Cond.	$A(y/n)$	Average PR	RMS PR
1	0.074	3.6	0.80
2	0.156	5.0	0.82
3	0.134	3.5	0.50
4	0.332	6.3	0.94
5	0.293	5.2	1.17

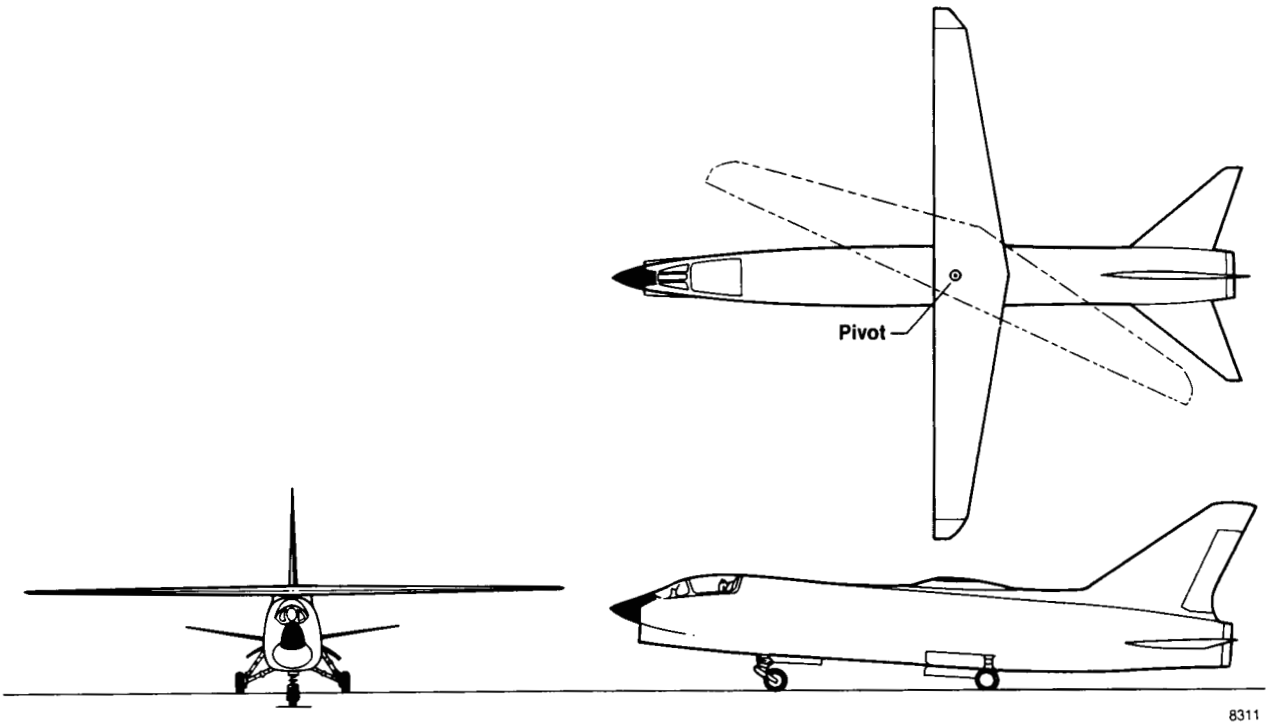

Figure 1. Three-view drawing of the oblique-wing research airplane.

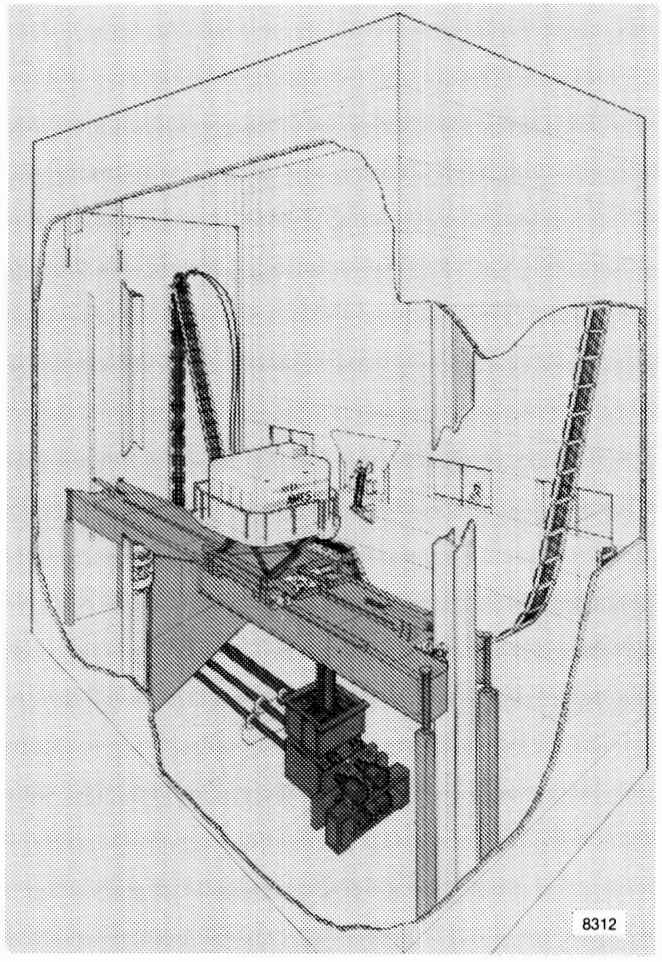

Figure 2. General view of the vertical motion simulator (VMS).

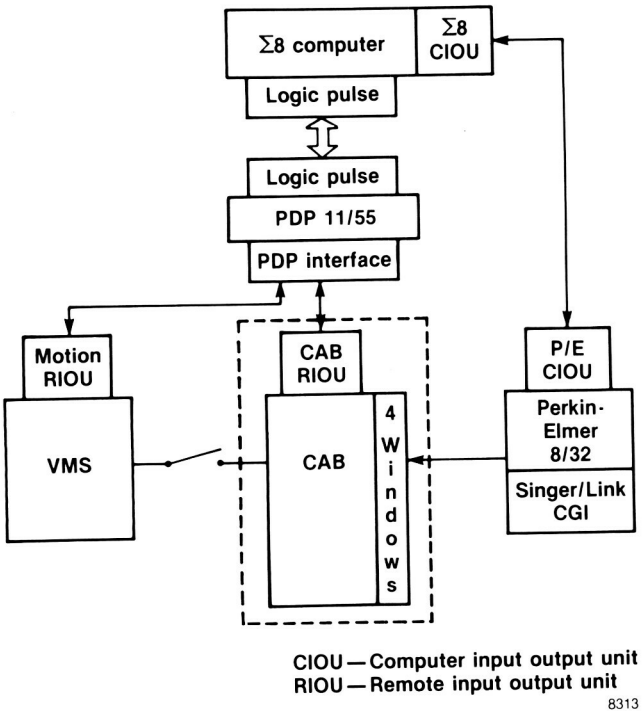

Figure 3. VMS system block diagram.

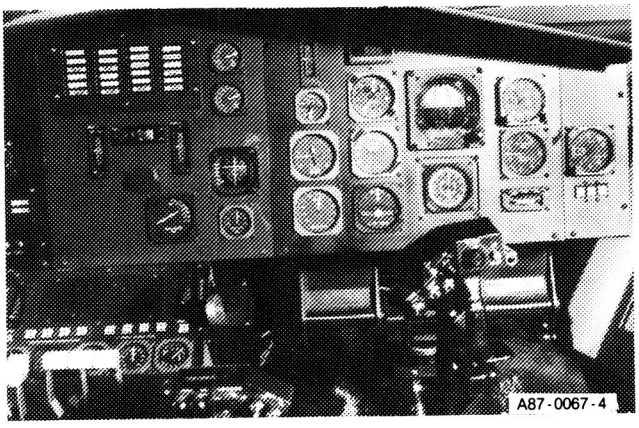

Figure 4. VMS cockpit arrangement.

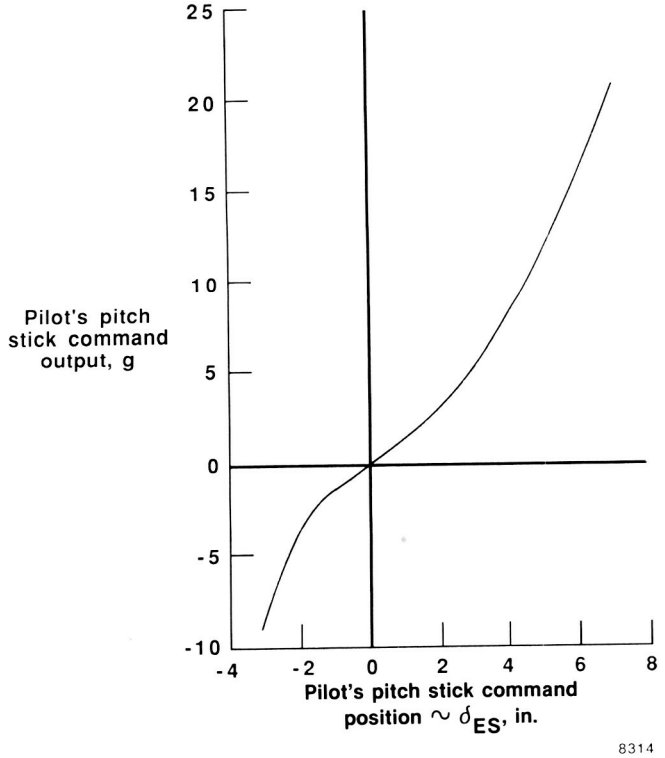

Figure 5. Nonlinear pitch stick characteristics used in the oblique-wing VMS.

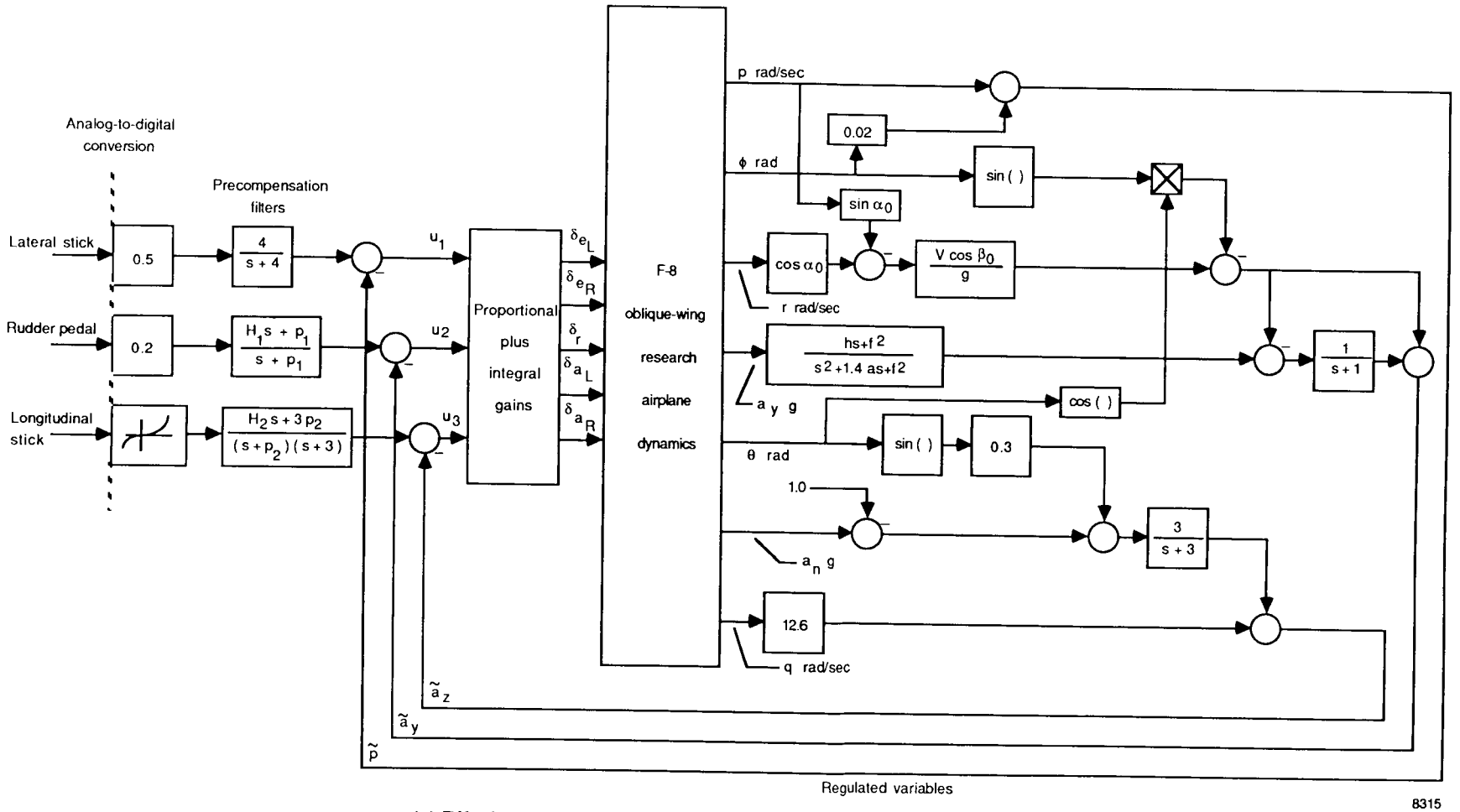

(a) Pilot's command inputs and formulation of regulated variables.

Figure 6. Preliminary control law used in the VMS study.

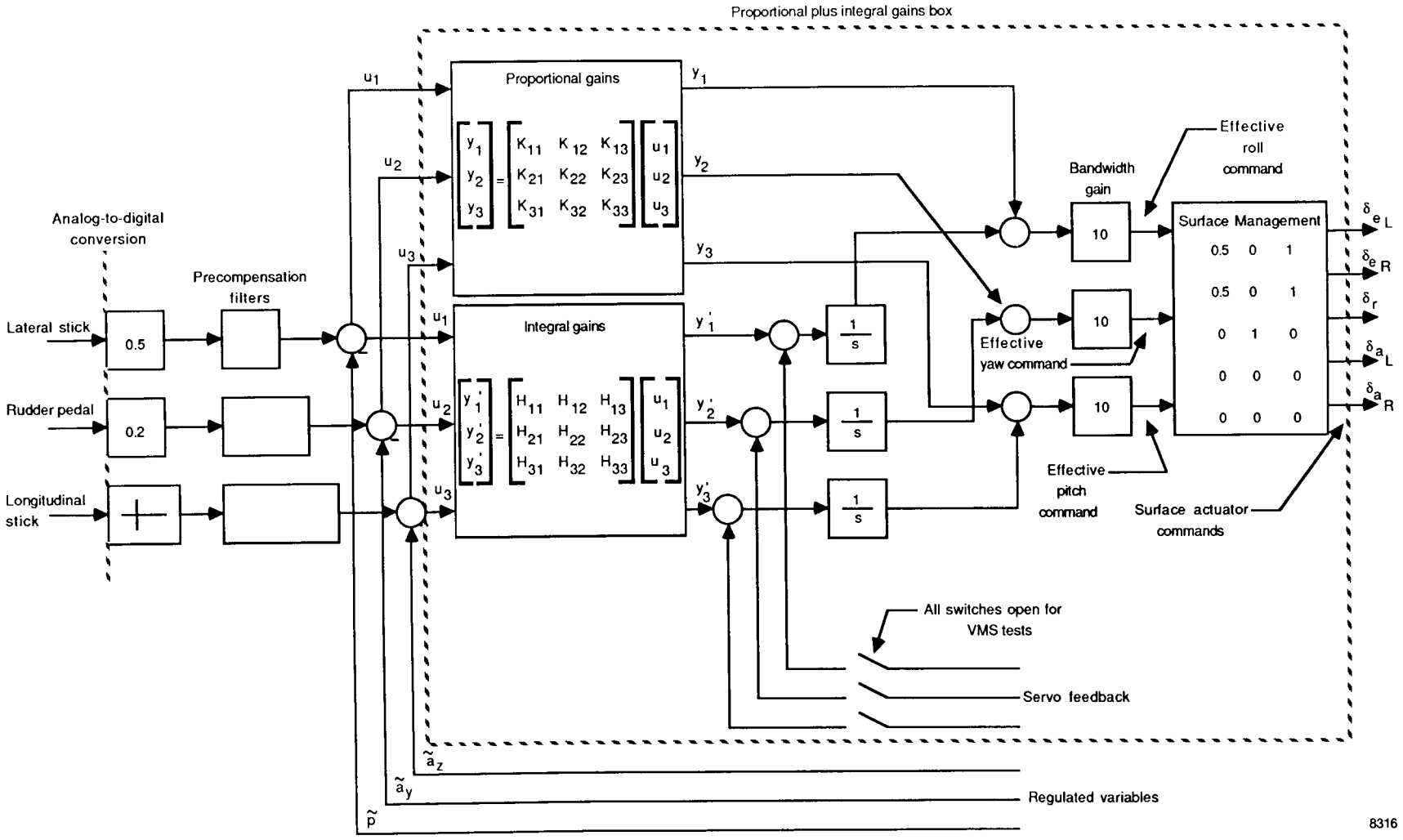

(b) Formulation of proportional and integral gains and surface management.

Figure 6. Continued.

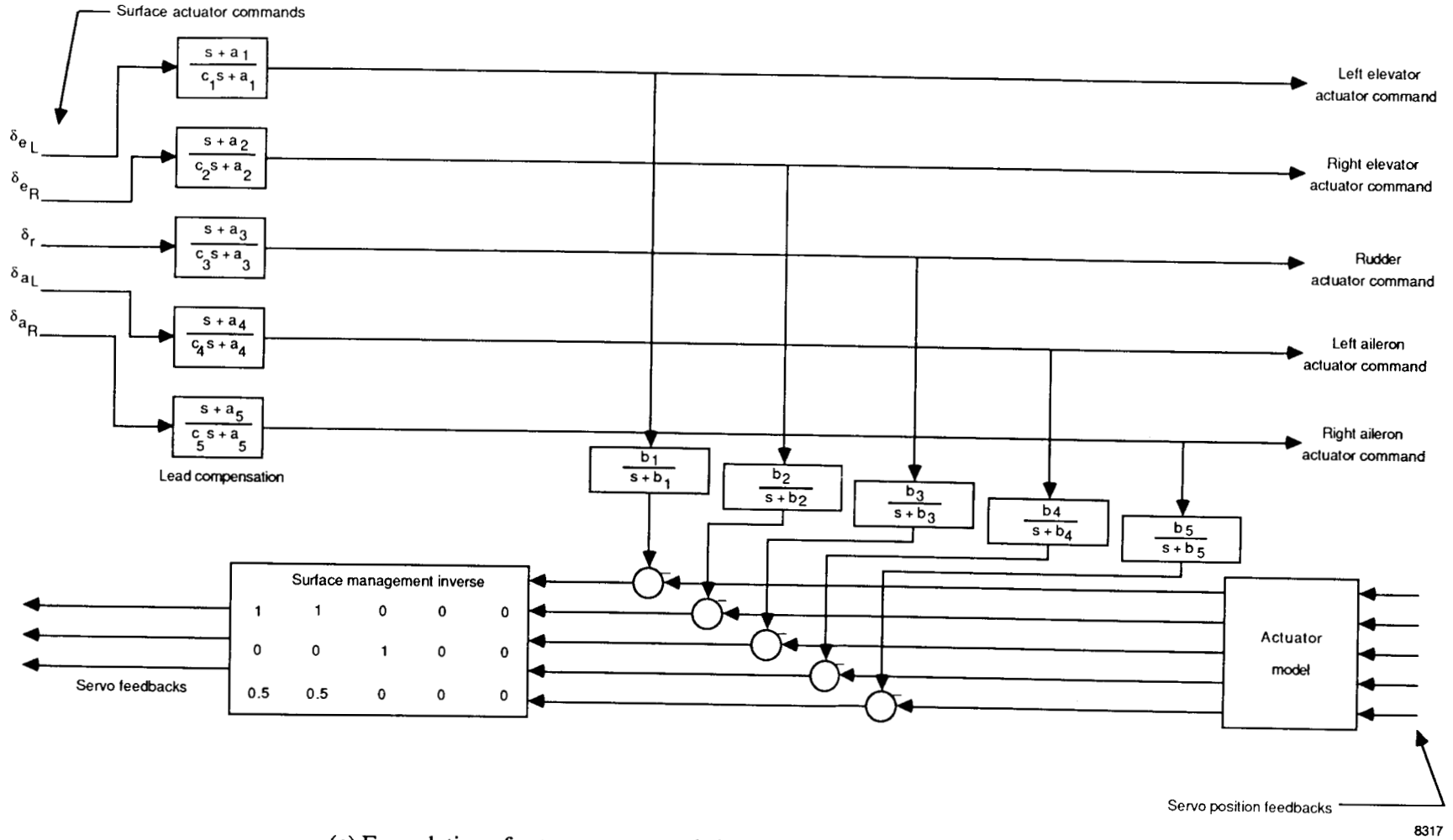

(c) Formulation of actuator command signals and servo feedback mechanization.

Figure 6. Concluded.

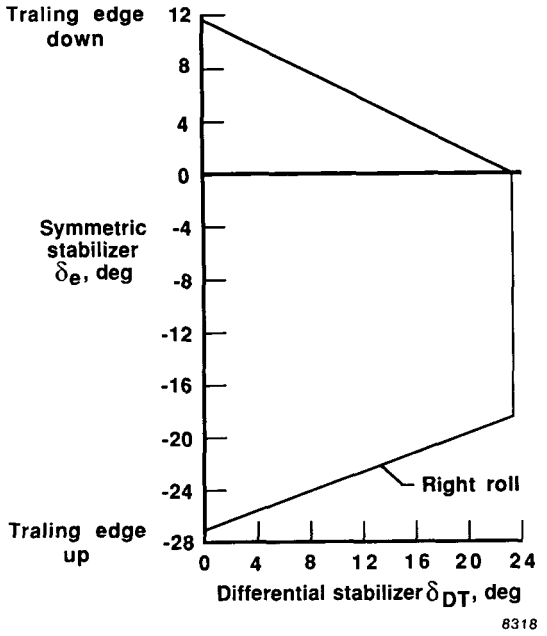

Figure 7. OWRA vertical motion simulation symmetric stabilizer and differential stabilizer position limit envelope.

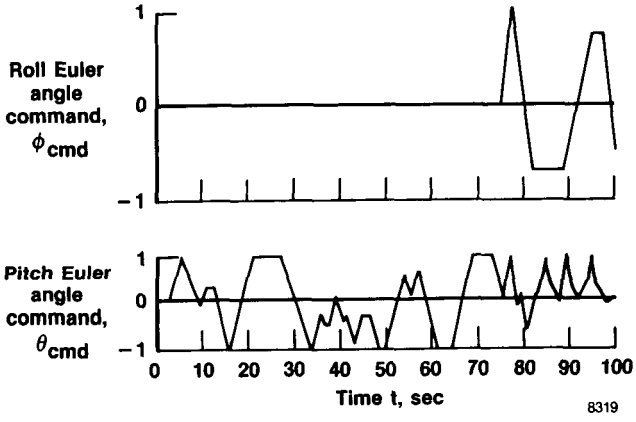

(a) Pitch with roll tracking.

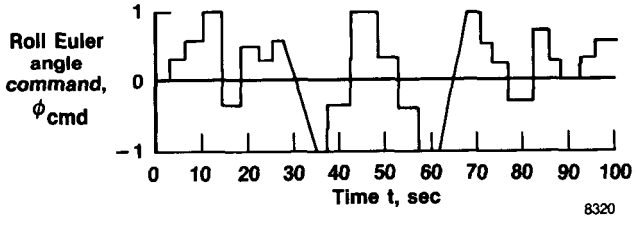

(b) Roll tracking task.

Figure 8. VMS OWRA command tracking task.

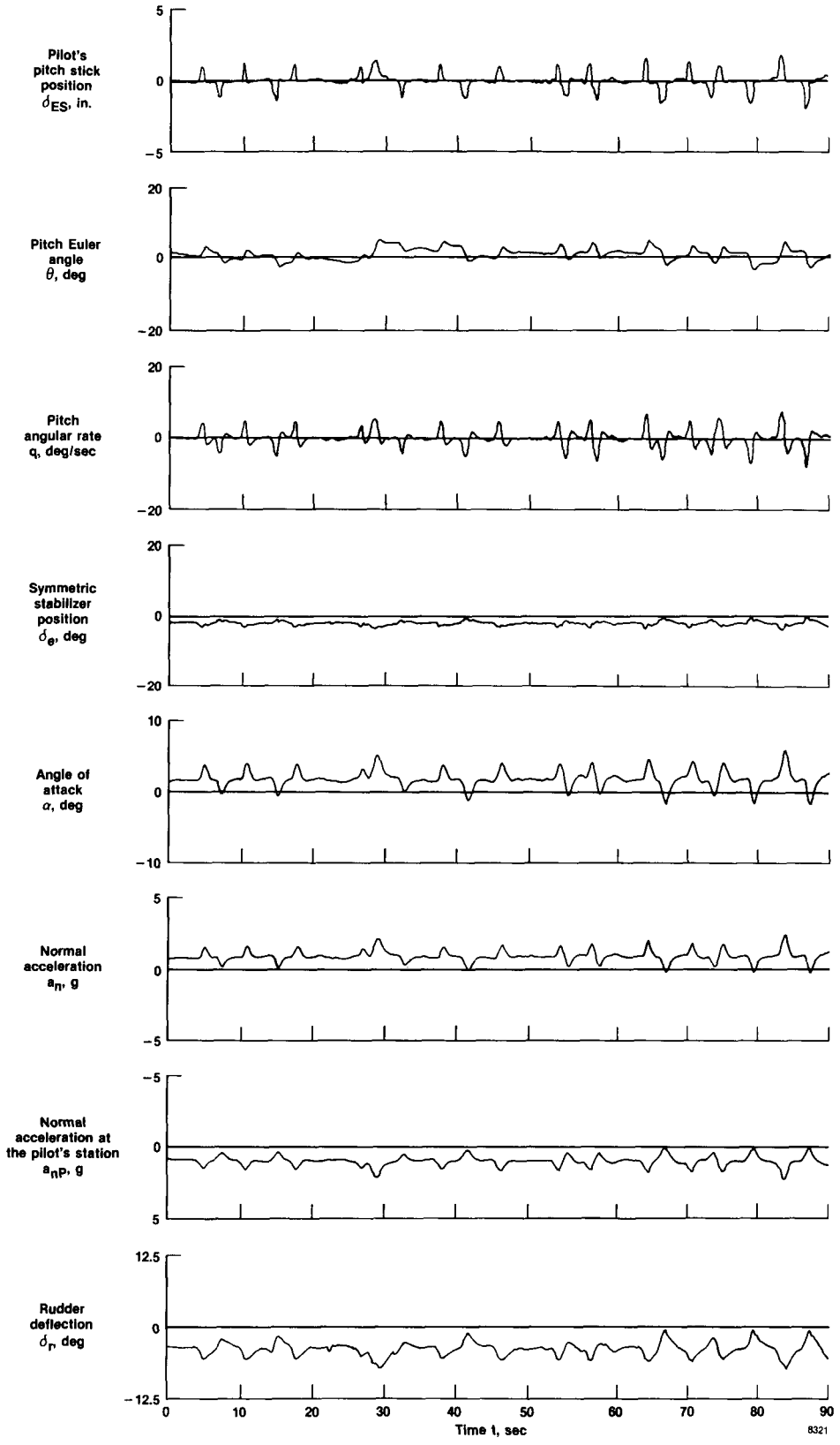

(a) Longitudinal parameters.

Figure 9. OWRA longitudinal and lateral-directional response parameters for small pitch pulses. $M = 0.8$, $h = 20,000$ ft, $\bar{q} = 436$ lb/ft^2, $\Lambda = 45°$

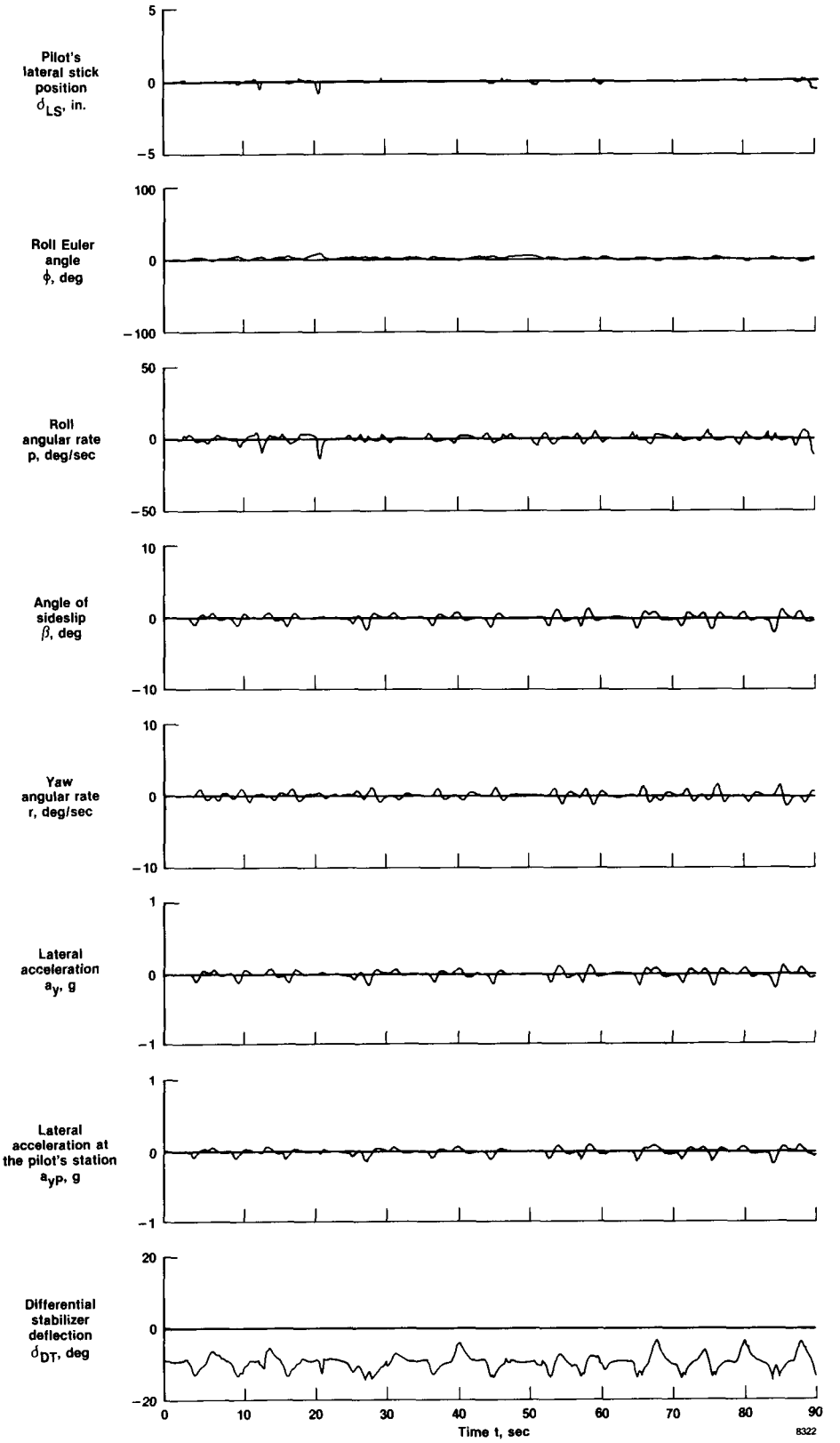

(b) Lateral-directional parameters.

Figure 9. Concluded.

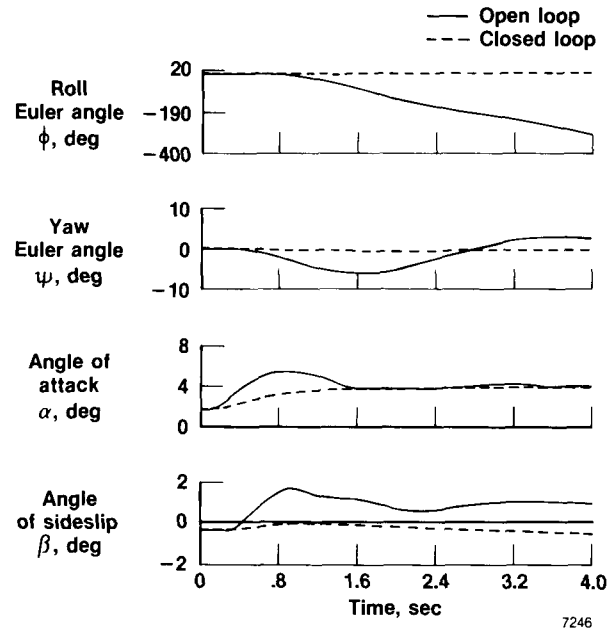

(a) Roll and yaw Euler angles, angle of attack, and angle of sideslip. Flight condition 1, $M = 0.8$, $h =$ 20,000 ft, $\Lambda = 45°$, $\bar{q} = 436.2$ lb/ft^2.

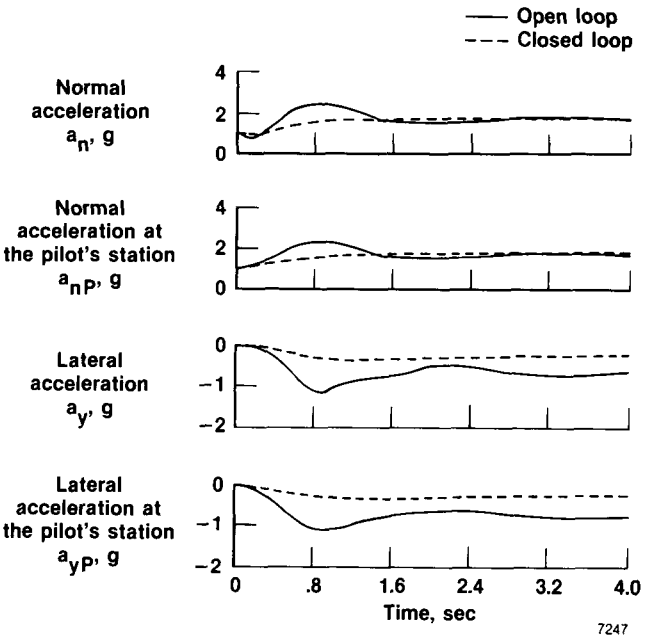

(b) Roll and yaw Euler angles, angle of attack, and angle of sideslip.

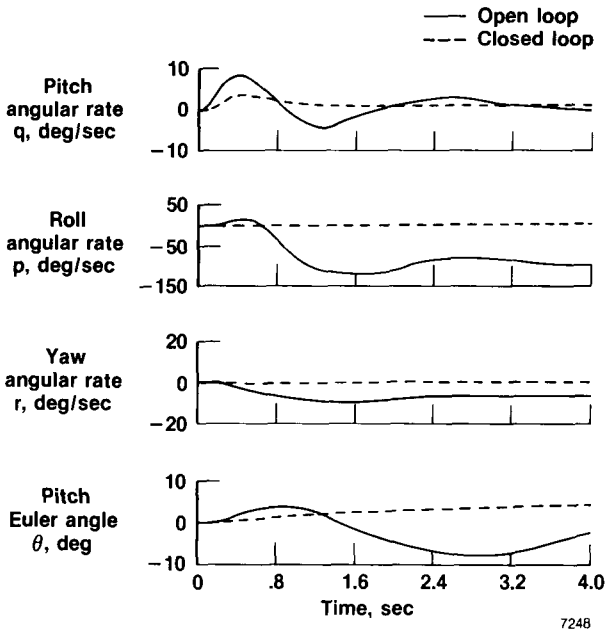

(c) Angular rates and pitch Euler angle.

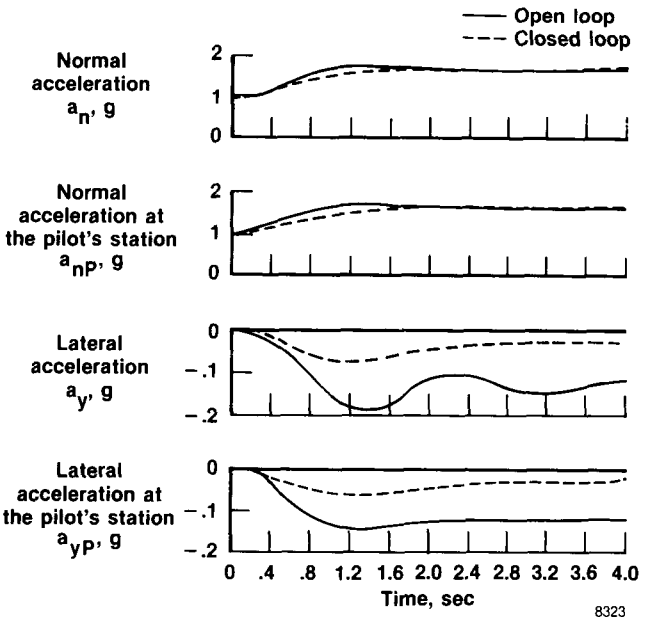

(d) Roll and yaw Euler angles, angle of attack, and angle of sideslip. Flight condition 4, $M = 1.6$, $h =$ 29,000 ft, $\Lambda = 65°$, $\bar{q} = 1181.4$ lb/ft^2.

Figure 10. OWRA open-loop and closed-loop nose up normal acceleration step command of approximately 2 g.

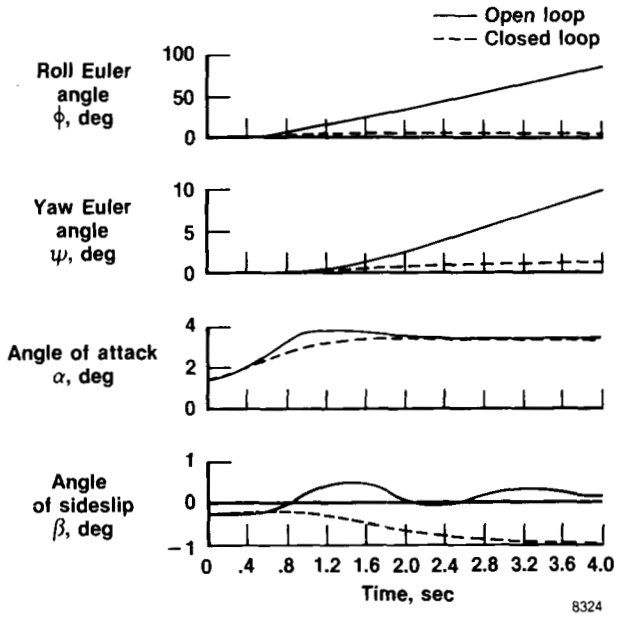

(e) Normal and lateral accelerations.

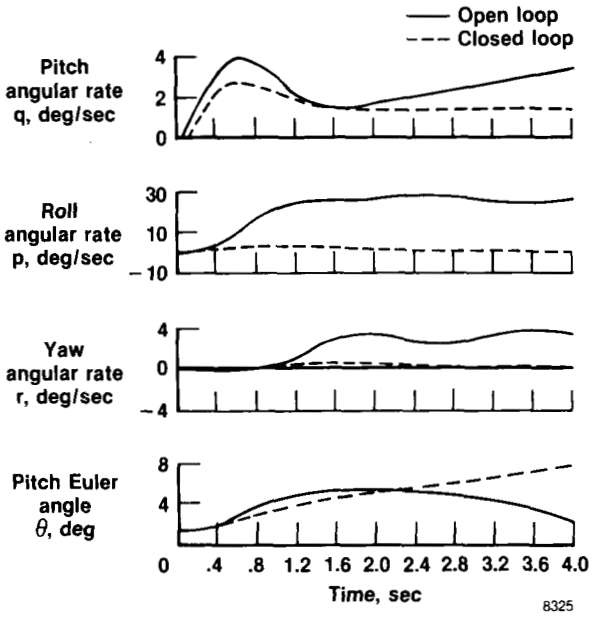

(f) Angular rates and pitch Euler angle.

Figure 10. Concluded.

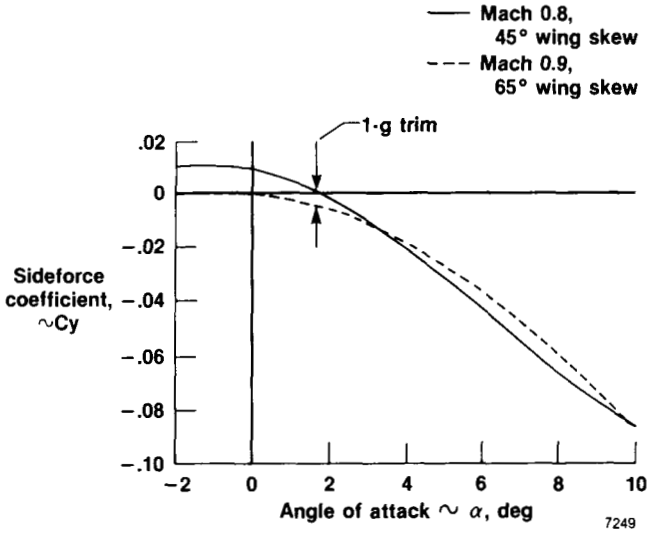

Figure 11. Wind-tunnel predictions of the OWRA sideforce coefficient as a function of angle of attack; $M = 0.8, \Lambda = 45°$, and $M = 0.9, \Lambda = 65°$.

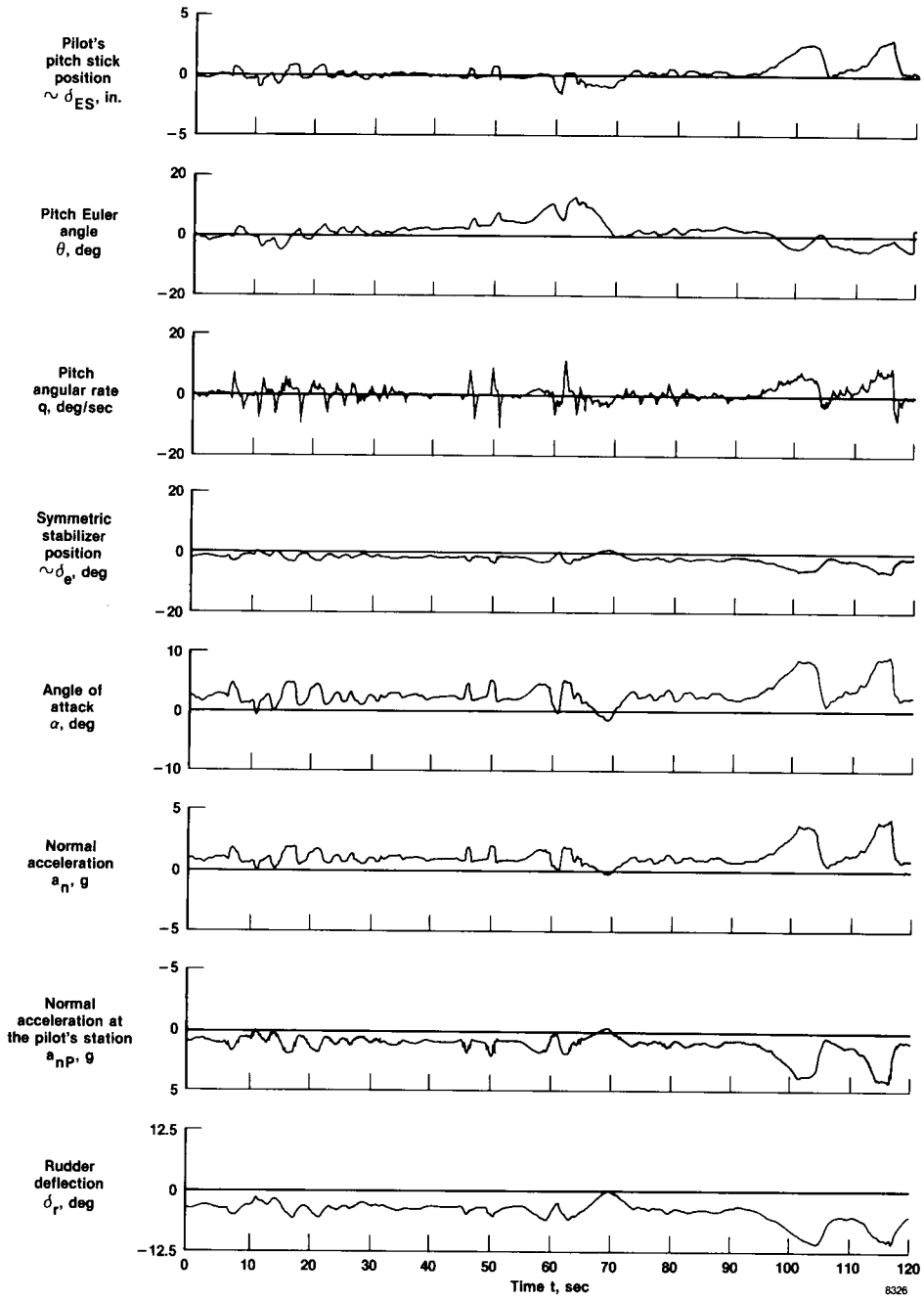

(a) Longitudinal parameters

Figure 12. OWRA longitudinal and lateral-directional response parameters for a pitch tracking task; M = 0.9, h = 500 ft, Λ = 65°, $\bar{q}$ = 1178.9 lb/ft^2.

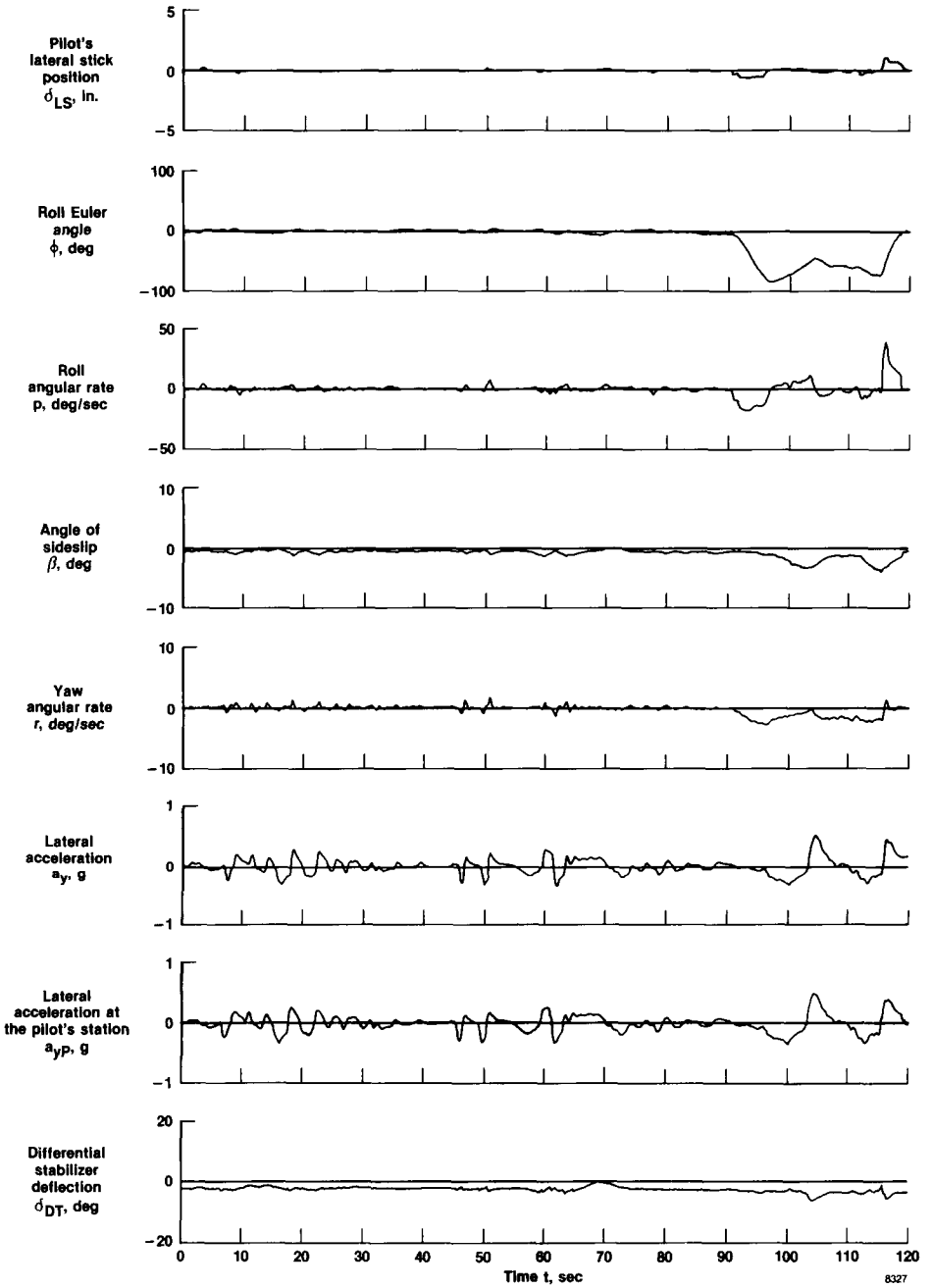

(b) Lateral directional parameters.

Figure 12. Concluded.

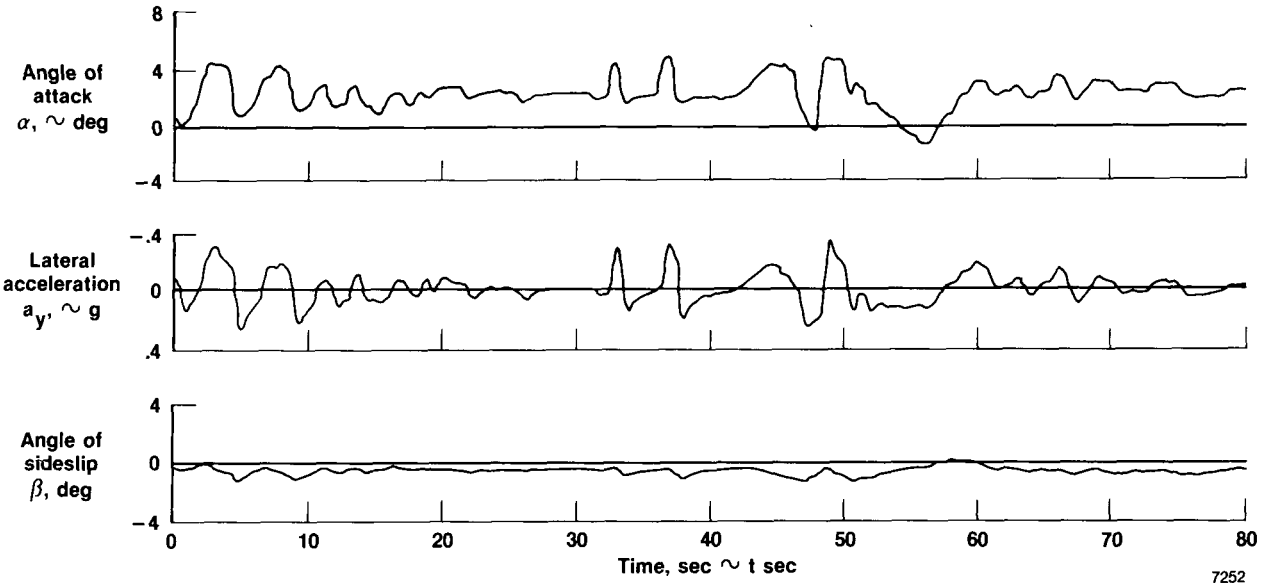

Figure 13. OWRA VMS time response comparison of angle of attack with lateral acceleration and angle of sideslip with no lateral pilot command inputs; $M = 0.9$, $\Lambda = 65°$, $\bar{q} = 1178.9$ lb/ft^2.

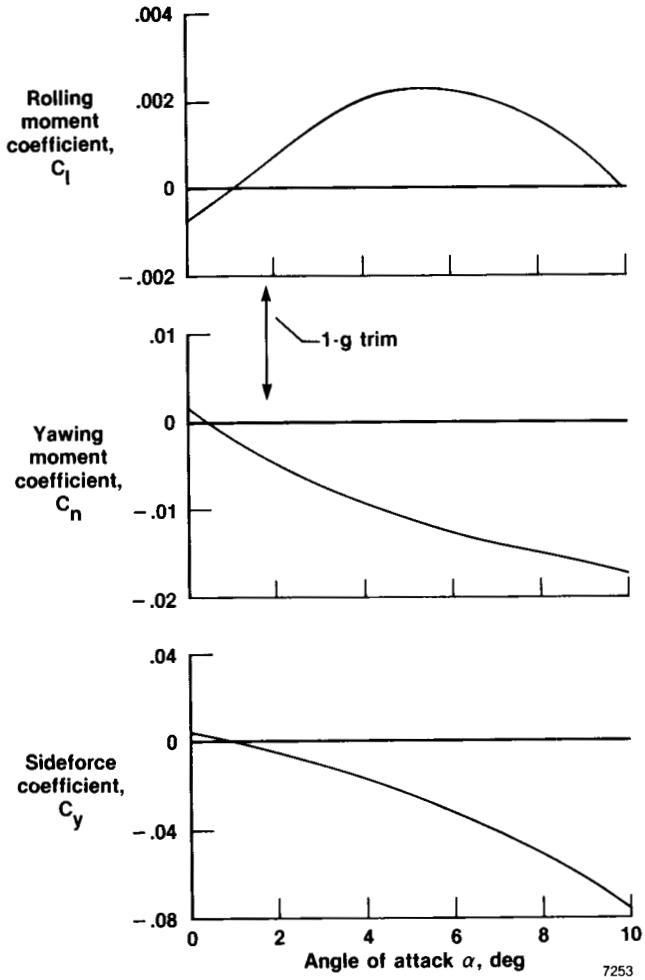

Figure 14. OWRA rolling and yawing moment, and sideforce coefficients. Flight condtion 4, $M = 1.6$, $\Lambda = 65°$.

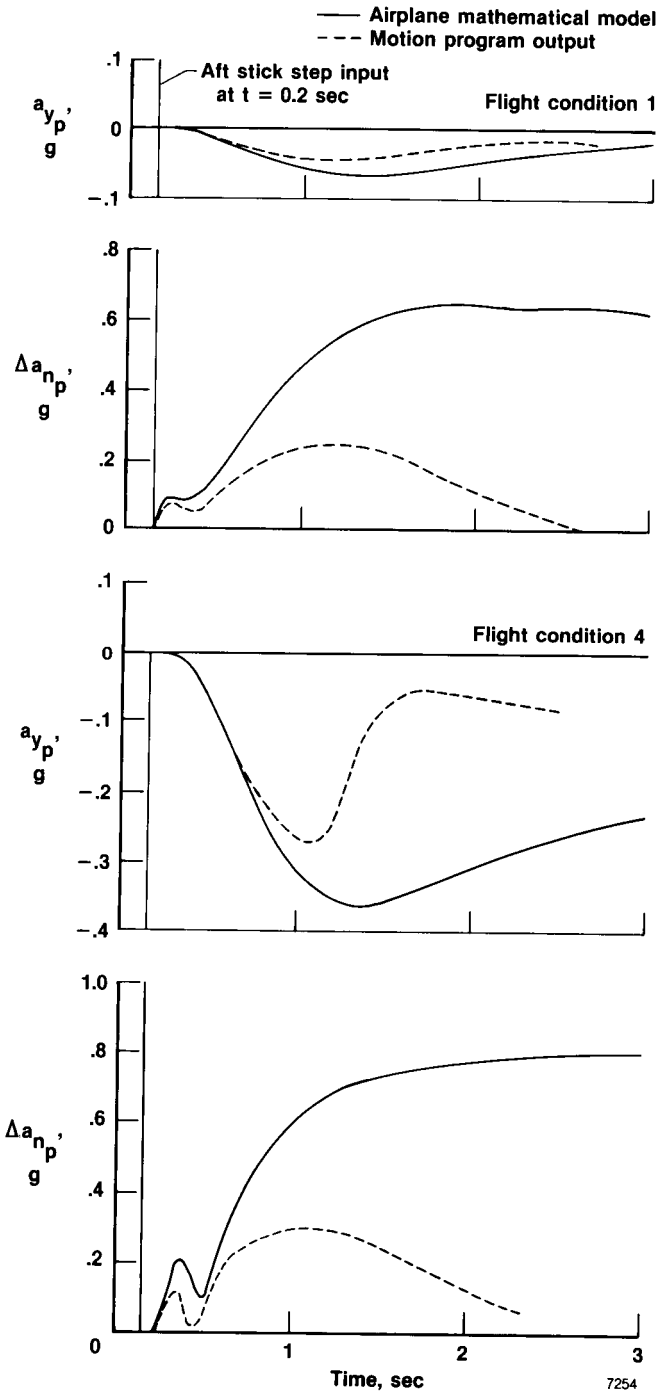

Figure 15. Cockpit side acceleration and normal acceleration responses to pitch step inputs for flight conditions 1 and 4.

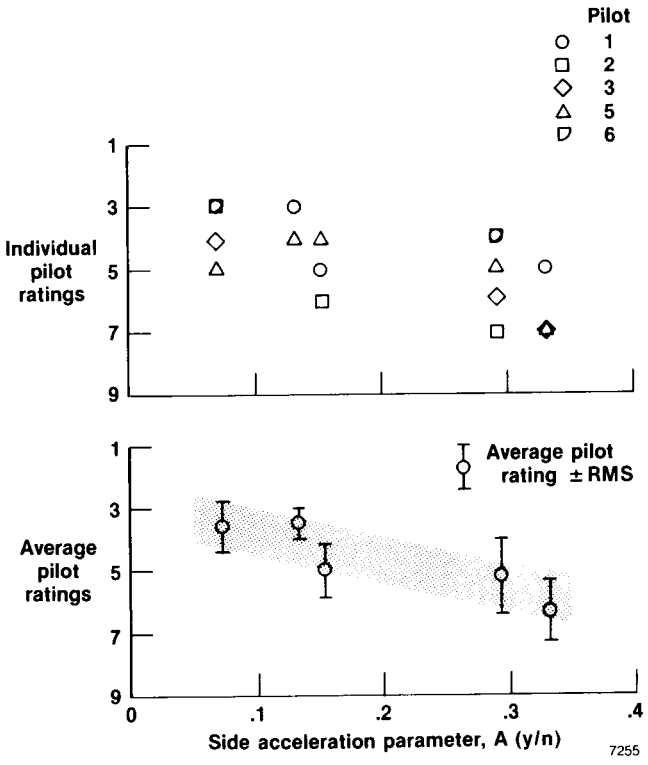

Figure 16. Pilot rating as a function of side-acceleration parameter for pitch maneuvering.

NASA
National Aeronautics and Space Administration

Report Documentation Page

1. Report No.	2. Government Accession No.	3. Recipient's Catalog No.
NASA TP-2874		

4. Title and Subtitle

A Piloted Evaluation of an Oblique-Wing Research Aircraft Motion Simulation With Decoupling Control Laws

5. Report Date

November 1988

6. Performing Organization Code

7. Author(s)

Robert W. Kempel, Walter E. McNeill, Glenn B. Gilyard, and Trindel A. Maine

8. Performing Organization Report No.

H-1430

10. Work Unit No.

RTOP 533-02-91

9. Performing Organization Name and Address

NASA Ames Research Center
Dryden Flight Research Facility
P.O. Box 273, Edwards, CA 93523-5000

11. Contract or Grant No.

13. Type of Report and Period Covered

Technical Paper

12. Sponsoring Agency Name and Address

National Aeronautics and Space Administration
Washington, DC 20546

14. Sponsoring Agency Code

15. Supplementary Notes

16. Abstract

The NASA Ames Research Center developed an oblique-wing research airplane from NASA's F-8 digital-fly-by-wire airplane. Oblique-wing airplanes show large cross-coupling in control and dynamic behavior which is not present in conventional symmetric airplanes and must be compensated for to obtain acceptable handling qualities. The large vertical motion simulator at NASA Ames-Moffett was used in the piloted evaluation of a proposed flight control system designed to provide decoupled handling qualities. Five discrete flight conditions were evaluated ranging from low altitude subsonic Mach numbers to moderate altitude supersonic Mach numbers. The flight control system was effective in generally decoupling the airplane. However, all participating pilots objected to the high levels of lateral acceleration encountered in pitch maneuvers. In addition, the pilots were more critical of left turns (in the direction of the trailing wingtip when skewed) than they were of right turns due to the tendency to be rolled into the left turns and out of the right turns. Asymmetric sideforce as a function of angle of attack was the primary cause of lateral acceleration in pitch. Along with the lateral acceleration in pitch, variation of rolling and yawing moments as functions of angle of attack caused the tendency to roll into left turns and out of right turns.

17. Key Words (Suggested by Author(s))	18. Distribution Statement
Asymmetric aircraft Flight controls Simulation	Unclassified — Unlimited Subject category 08

19. Security Classif. (of this report)	20. Security Classif. (of this page)	21. No. of pages	22. Price
Unclassified	Unclassified	52	A04

NASA FORM 1626 OCT 86

**For sale by the National Technical Information Service, Springfield, VA 22161-2171.*

NASA-Langley, 1988